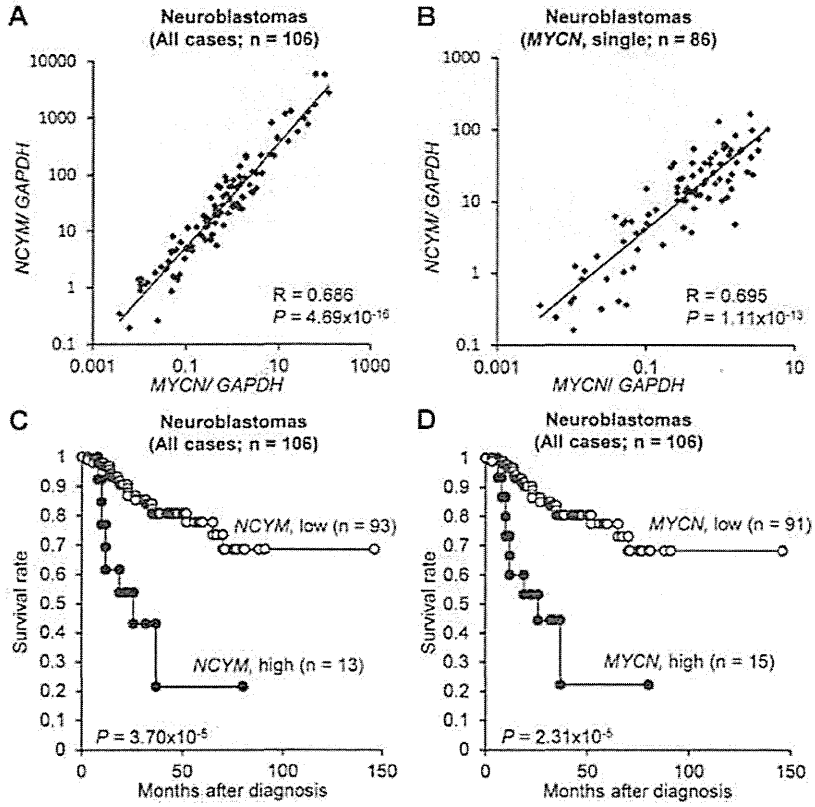

Figure 2. *NCYM* expression is associated with poor prognosis in human neuroblastoma. (A) *NCYM* mRNA expression correlates with that of *MYCN* in human primary neuroblastomas (n = 106, Rs. = 0.686, $P = 4.69 \times 10^{-16}$). (B) *NCYM* mRNA expression correlates with that of *MYCN* in human primary neuroblastomas with *MYCN* single copy (n = 86, Rs. = 0.695, $P = 1.11 \times 10^{-13}$). The mRNA expression of *NCYM* and *MYCN* was detected by qRT-PCR and normalized using *GAPDH*. (C) Kaplan–Meier survival curves (n = 106, $P = 3.70 \times 10^{-5}$, log-rank test). The expression levels of *NCYM* were designated high (n = 13, closed circle) or low (n = 93, open circle) based on the respective average expression. (D) Kaplan–Meier survival curves. The expression levels of *MYCN* were designated high (n = 15, closed circle) or low (n = 91, open circle) based on the respective average expression. High *MYCN* mRNA expression was significantly correlated with poor prognosis (n = 106, $P = 2.31 \times 10^{-5}$, log-rank test).
doi:10.1371/journal.pgen.1003996.g002

to its proteasome-dependent protein degradation after an E3-mediated polyubiquitination [28,29]. Therefore, using immunoprecipitation, we next searched for factors interacting with NCYM that are able to induce MYCN stabilization, and found that NCYM forms a complex with MYCN and GSK3β in CHP134 cells (Figure 3F and G). In addition, purified NCYM was capable of interacting with purified GSK3β and MYCN *in vitro* (Figure 3H). To examine the effect of NCYM on GSK3β-mediated phosphorylation of MYCN, we performed an *in vitro* kinase assay (Figure 3I). NCYM protein inhibited the phosphorylation of MYCN. Because the purified NCYM protein is not a substrate of GSK3β (Figure S12), it is unlikely that NCYM competes with MYCN for GSK3β as a substrate. Taken together these results suggest that the NCYM protein inhibits GSK3β-mediated MYCN phosphorylation and stabilizes the MYCN protein *in vitro*.

It has been reported that MYCN knockdown decreases cell proliferation and induces apoptosis and/or differentiation in *MYCN*-amplified neuroblastoma cells [30]. Therefore, we next investigated the functional role of NCYM in these cells (Figure S13 and S14). We performed NCYM knockdown in BE (2)-C, CHP134, SK-N-AS and SH-SY5Y human neuroblastoma cells. SK-N-AS and SH-SY5Y cells are *MYCN*-single copy but have a high expression of *MYC*, while BE (2)-C and CHP134 are cell lines with *MYCN*-amplification and hence have a high expression of *MYCN* and *NCYM* (Figure S13A). NCYM knockdown did not affect the survival of the *MYCN*-single neuroblastoma cell lines, but promoted massive apoptosis of the *MYCN*-amplified neuroblastoma cells (Figure S13B and C). In addition, in BE (2)-C cells, NCYM knockdown was found to inhibit cell proliferation and invasion (Figure S14B and D). These results suggest that NCYM promotes the survival and aggressiveness of *MYCN*-amplified neuroblastoma cells.

Co-expression of *MYCN/NCYM* in mice promotes neuroblastoma metastasis

To assess the function of NCYM *in vivo*, we generated transgenic mice expressing the human *NCYM* gene under the control of the rat *tyrosine hydroxylase* (*TH*) promoter (Figure S15A and B). In addition, we made double transgenic mice carrying both the human *MYCN* and *NCYM* genes. *NCYM* Tg/+ mice were mated with *MYCN* Tg/+ *NCYM* Tg/+ mice, and 83 descendants were observed for 200 days (Figure S15C and D). None of the *NCYM* transgenic mice of the 129^{+tet}/SVJ background developed neuroblastoma (Figure S15D), suggesting that NCYM overexpression alone is not sufficient to initiate neuroblastoma *in vivo*. Although tumor formation was not accelerated in the *MYCN/*

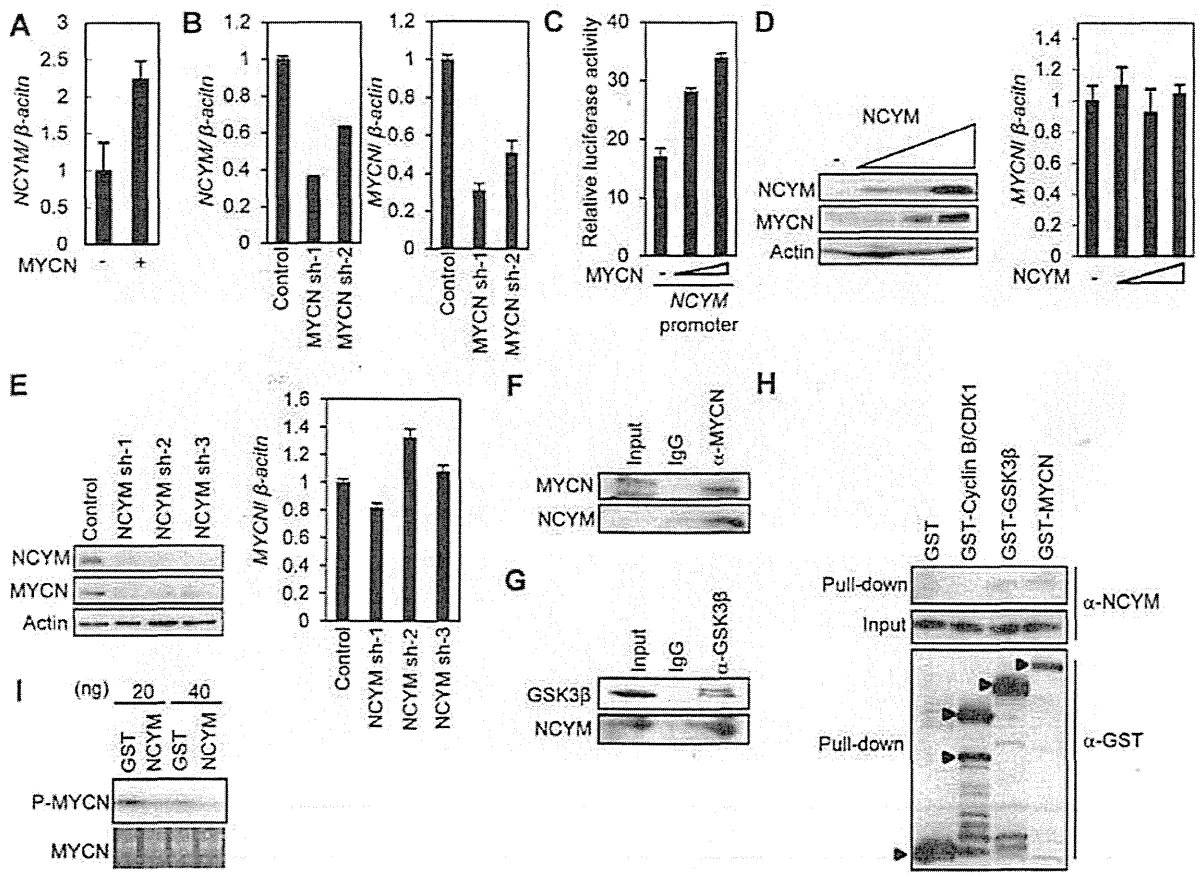

Figure 3. Functional interaction between NCYM and MYCN. (A) Relative mRNA levels of *NCYM* in SK-N-AS *MYCN* single copy human neuroblastoma cells transfected with MYCN expression vector. mRNA levels were measured by qRT-PCR with *β-actin* as an internal control. (B) Relative mRNA levels of *NCYM* (left panel) or *MYCN* (right panel) upon depletion of MYCN in CHP134 human *MYCN*-amplified neuroblastoma cells. (C) MYCN enhances *NCYM* promoter activity. Human neuroblastoma SK-N-AS cells were transfected with increasing amounts of MYCN expression plasmid (0, 200, 300 ng) and their luciferase activity was measured. (D) Western blots showing NCYM overexpression induces MYCN protein in Neuro 2a mouse neuroblastoma cells (left panel). *MYCN* mRNA expression in mouse neuroblastoma Neuro 2a cells transfected with increasing amounts of NCYM expression vector measured by qRT-PCR (right panel). (E) Western blots showing NCYM knockdown decreases MYCN protein in CHP134 cells (left panel). *MYCN* mRNA expression in NCYM knockdown CHP134 cells as measured by qRT-PCR (right panel). (F, G) Co-immunoprecipitation of endogenous NCYM with endogenous MYCN and GSK3β. (H) GST-pulldown assay. Purified NCYM proteins were pulled down with GST-fused GSK3β and MYCN. (I) *In vitro* kinase assay. Radiolabeled ATP was used for the second reaction with GSK3β together with the indicated amount of NCYM or GST. The amount of phosphorylated MYCN was quantified using standard autoradiography. The total amount of the MYCN was quantified by using an Oriole Fluorescent Gel stain.
doi:10.1371/journal.pgen.1003996.g003

NCYM double transgenic mice (Figure S15E), the incidence of neuroblastomas with distant metastases was significantly increased in the *MYCN/NCYM* double transgenic mice (Figure 4, Figure S16, Table S3). The overexpression of the MYCN and NCYM proteins in primary and metastatic tumor cells was confirmed by immunohistochemistry (Figure 4B). In the neuroblastoma tissue of the double transgenic mice, GSK3β was significantly inactivated by phosphorylation at serine 9 (Figure 5A). To investigate the mechanism by which NCYM promotes the phosphorylation of GSK3β, we analyzed the phosphorylation status of the known upstream kinases for GSK3β, AKT [28] and S6K [31]. S6K was highly phosphorylated in the *MYCN/NCYM* double transgenic mice, whereas AKT was not noticeably activated. The phosphorylation levels of S6K in neuroblastomas from the *MYCN/NCYM* double transgenic mice were correlated with the expression levels of MYCN and NCYM (Figure 5A, M7-M11). These results suggest that NCYM promotes the phosphorylation of GSK3β via the activation of mTOR-S6K signaling. Furthermore, NCYM co-immunoprecipitated with GSK3β (Figure 5B) and substrates of GSK3β such as MYCN and β-catenin were stabilized in the neuroblastoma tissues induced in *MYCN/NCYM* transgenic mice (Figure 5A). We next examined the number of apoptotic cells in neuroblastomas from *MYCN* transgenic mice and *MYCN/NCYM* double transgenic mice by staining for cleaved caspase-3 (Figure S17). The number of apoptotic tumor cells was significantly decreased in the primary tumors of *MYCN/NCYM* double transgenic mice, suggesting that NCYM promotes the survival of neuroblastoma cells *in vivo*.

The tumors which develop in *MYCN/NCYM* transgenic mice are resistant to PI3K/mTOR inhibition

To examine whether the overexpression of NCYM contributes to the chemosensitivity of neuroblastomas via GSK3β inhibition, we tested the effect of NVP-BEZ235 on the survival of the *MYCN/*

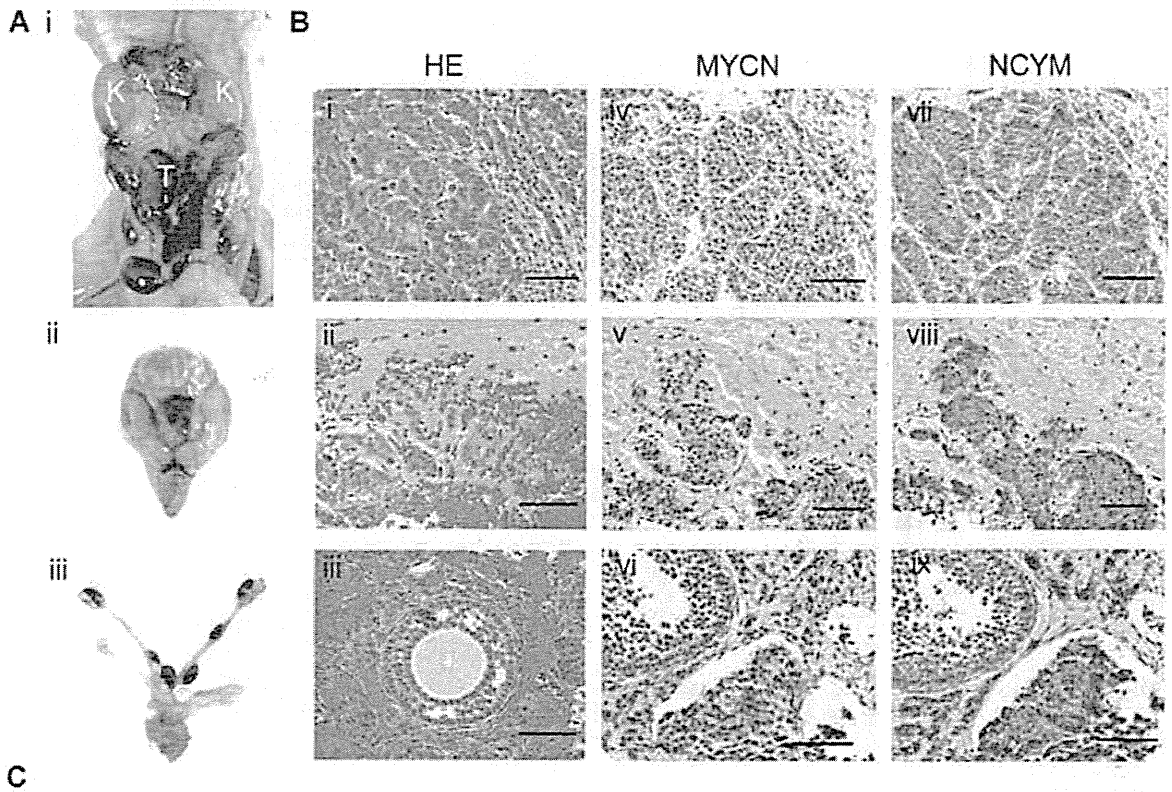

C

Metastatic tumor	*MYCN* Tg/+	*MYCN* Tg/+ *NCYM* Tg/+		*MYCN* Tg/+ *NCYM* Tg/Tg
		Line 4	Line 6	Line 6
No	21	2	12	7
Yes	1 (4.5%)	4 (67%)	5 (29%)	3 (30%)
Total	22	6	17	10

Figure 4. NCYM promotes metastasis in mouse transgenic models of neuroblastoma. (A) Neuroblastomas arise as multifocal primary lesions in a *MYCN/NCYM* double transgenic mouse (line 6). (i) Abdominal primary tumors and metastatic tumors in the intracranium (ii) and ovary (iii) occurred within the same mouse (M1). (B) H&E staining (i, ii, iii) and immunohistochemistry for MYCN (iv, v, vi) and NCYM (vii, viii, ix) expression in abdominal tumors (i, iv, vii) and metastatic tumors in the intracranium (ii, v, viii) and ovary (iii, vi, ix), in the MYCN/NCYM transgenic mouse (M1). Scale bars, 50 μm. (C) The rates of metastatic tumor development in *MYCN* and *MYCN/NCYM* transgenic mice. Line 6; $P = 0.036$, Mann–Whitney U test. Line 4; $P < 0.01$, Fisher's exact probability test.
doi:10.1371/journal.pgen.1003996.g004

NCYM double transgenic mice. NVP-BEZ235 is a dual inhibitor of both PI3K and mTOR and promotes the degradation of MYCN to effectively reduce tumor burden in the *MYCN* transgenic mouse via GSK3β activation [32]. As reported, NVP-BEZ235 treatment significantly prolonged the survival duration of the *MYCN* transgenic mice ($P < 0.01$; Figure 5C). In contrast NVP-BEZ235 did not prolong the survival of the *MYCN/NCYM* double transgenic mice ($P = 0.648$; Figure 5D). Thus, the expression of NCYM reduced the efficiency of this drug *in vivo*.

Discussion

Our results reveal that *NCYM*, which was initially thought to be a large non-coding RNA transcribed from a *cis*-antisense gene of human *MYCN* [26], is actually translated into a functional protein in humans. *MYCN* is a highly conserved, major oncogene in human cancer. The newly evolved *cis*-antisense *NCYM* gene product targets the sense *MYCN* gene product, influencing its stabilization, which in turn enhances transcription of the *NCYM* gene. This positive autoregulatory loop may function in primary human neuroblastomas to enhance metastasis as well as drug resistance through stabilization of MYCN and even β-catenin, which are mediated by inhibition of GSK3β (Figure S18). Thus, NCYM is the first *de novo* evolved gene product shown to function in the development of human neuroblastoma.

NCYM promoted phosphorylation of GSK3β at serine 9 possibly via the activation of mTOR-S6K signaling, that might have led to the constitutive inactivation of GSK3β *in vivo*.

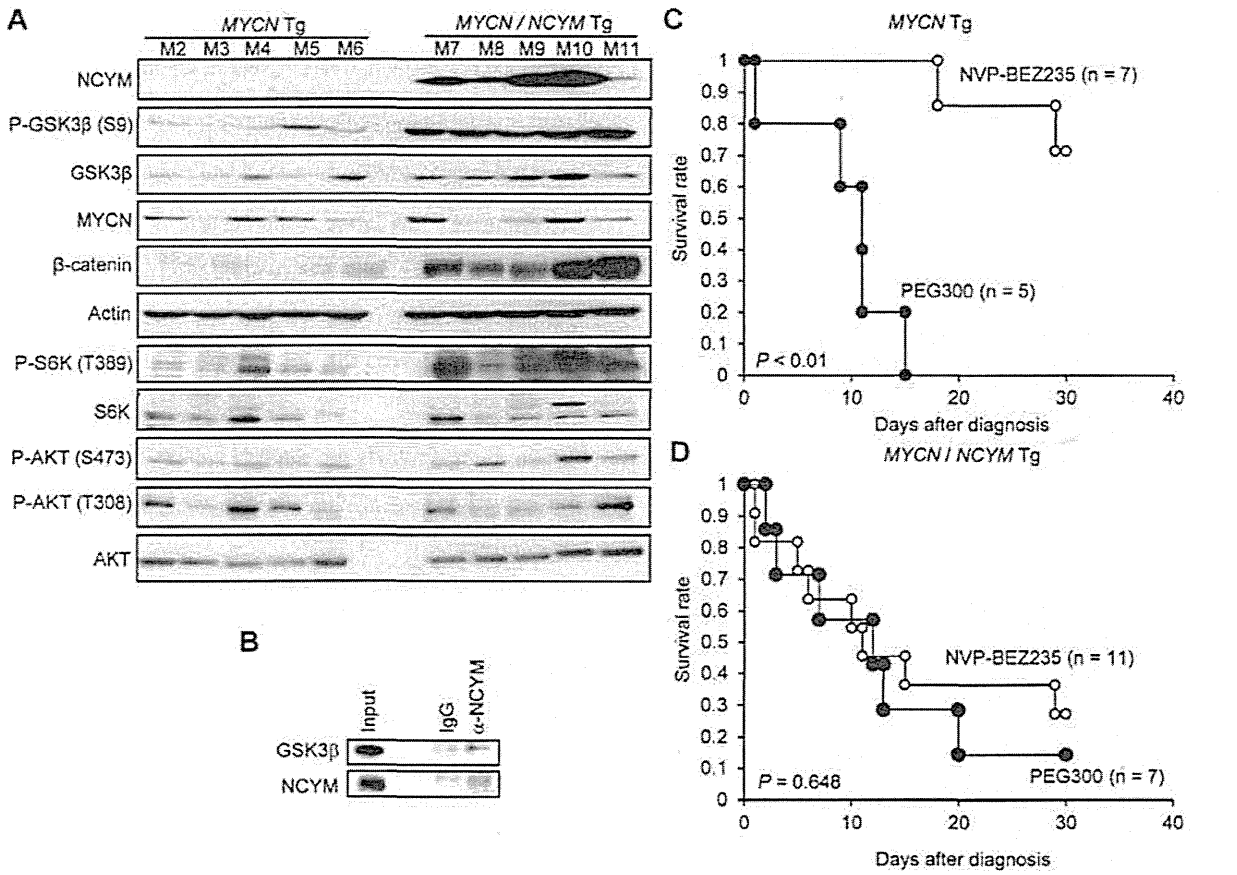

Figure 5. *MYCN/NCYM* tumors show drug resistance to a PI3K/mTOR-dual inhibitor. (A) Western blots of *MYCN* (M2–M6) and *MYCN/NCYM* (M7–M11) mouse tumors for NCYM, phospho-GSK3β (S9), GSK3β, β-catenin, and MYCN, phospho-S6K (T389), S6K, phospho-AKT (S473), phospho-AKT (T308), and AKT. *Actin* was used as loading control. (B) NCYM binds to GSK3β *in vivo*. Tumors developed in *MYCN/NCYM* transgenic mice (M12) were immunoprecipitated with control IgG or NCYM antibodies. GSK3β was co-immunoprecipitated with a NCYM antibody. (C, D) Kaplan–Meier survival analysis of *MYCN* mice (panel C, $P<0.01$, log-rank test) or *MYCN/NCYM* mice (panel D, $P=0.648$, log-rank test). Treatment with NVP-BEZ235 (35 mg/kg; open circles) or vehicle (PEG300; closed circles). NVP-BEZ235, *MYCN* transgenic mice n = 7, *MYCN/NCYM* transgenic mice n = 11; PEG300, *MYCN* transgenic mice n = 5, *MYCN/NCYM* transgenic mice n = 7.
doi:10.1371/journal.pgen.1003996.g005

Recently, Schramm *et al.* reported that MYCN transcriptionally regulates the mTOR pathway, promoting its activation [33]. Thus, MYCN might have enhanced S6K phosphorylation by activating the mTOR pathway in neuroblastomas caused in the double transgenic mice. Previous reports have suggested that neuroblastoma cell lines expressing high levels of MYCN were significantly more sensitive to mTOR inhibitors compared with cell lines expressing low MYCN levels [34]. Furthermore, our study showed that NCYM knockdown significantly induces apoptosis in *MYCN*-amplified neuroblastoma cells, whereas the effects were marginal in *MYCN*-single neuroblastoma cells. Therefore, the feedback regulation between mTOR-S6K signaling and MYCN/NCYM may contribute to the survival of *MYCN*-amplified neuroblastoma cells (Figure S18).

Although NCYM inhibits GSK3β-mediated MYCN phosphorylation *in vitro*, our data does not rule out the possibility that NCYM may stabilize MYCN in a GSK3β-independent manner. Because NCYM binds directly to MYCN both *in vitro* and in neuroblastoma cells, this may affect the recruitment of the regulators of MYCN stability. Indeed, we have recently found that the tumor suppressor protein Runx3 directly binds to MYCN in neuroblastoma cells and promotes degradation of MYCN in the ubiquitin–proteasome system dependent manner [35]. Therefore, the binding of NCYM to MYCN itself could affect the interaction of Runx3, or other regulators such as Aurora A [36] with MYCN to induce its stability. Further studies are required to evaluate the role of NCYM-mediated inhibition of GSK3β activity on MYCN stability.

Recent reports have suggested that both mutant ALK [37,38] and Lin28B [39] promote the growth of neuroblastomas in transgenic mouse models by targeting MYCN for stabilization [37,38] or overexpression [39]. Among the known regulators of MYCN, *NCYM* is the only gene that shows 100% co-amplification with *MYCN* in human primary neuroblastomas. Overexpressed NCYM stabilizes both MYCN and β-catenin, and enhances the generation of neuroblastomas with increased aggressive behavior such as distant metastasis and/or drug resistance, which are characteristics reminiscent of human neuroblastoma. Recently, Valentijn *et al.* suggested that the activation of the MYCN pathway is a more significant prognostic factor than the expression or amplification of MYCN in primary neuroblastomas [40]. Consistent with this, our results indicate that *NCYM* expression is

associated with poor outcomes in human neuroblastoma regardless of genomic status of the *MYCN/NCYM* locus. Therefore, we anticipate that the positive auto-regulatory loop formed by MYCN and NCYM may be a promising target for developing novel therapeutic tools against high-risk neuroblastoma.

As suggested in the recent report [37], the concomitant inhibition of apoptosis and/or activation of survival signals may be required for MYCN to induce multiple tumors or metastases *in vivo*. In this study, we found that NCYM maintains the survival of *MYCN*-amplified neuroblastoma cells, and that the apoptotic cell number, indicated by cleaved caspase-3, was downregulated in *MYCN/NCYM* transgenic mice. In addition, GSK3β inhibition contributes to the inhibition of apoptosis in response to treatment with DNA-damaging drugs in neuroblastoma cells [41]. Therefore, the concomitant activation of other GSK3β substrates, such as β-catenin, and mTOR-S6K signaling by NCYM may be involved in the inhibition of apoptosis (Figure S18).

Since the proposals of Ohno and Jacob, the birth of a new gene has been believed to be caused by the duplication or rearrangement of pre-existing genes [1,2]. The recent advances in whole genome sequencing technology and bioinformatics have identified the presence of *de novo* proteins; however, their physiological or pathological significance have largely remained unclear [3,15]. In 2010, Li *et al.* reported that MDF1 originated *de novo* from a DNA sequence previously thought to be non-coding in *Saccharomyces cerevisiae* [7]. MDF1 inhibits mating efficiency by binding MATα2 and promoting vegetative growth. Therefore, while MDF1 was the first reported *de novo* gene whose protein product function was unveiled in a monad, NCYM may be the first *de novo* protein whose precise function has been clarified in multicellular organisms, specifically in humans.

In conclusion, NCYM is a *de novo* evolved protein which acts as an oncopromoting factor in human neuroblastoma. Our results suggest that *de novo* evolved new gene products may be involved in the functional regulation of human cancers and even other diseases.

Materials and Methods

Evolutionary analyses

DNA sequences of all species were extracted from the UCSC genome browser on the basis of conservation. From the protein-coding regions, we took the conserved block that was annotated as the region corresponding to the *NCYM* coding sequence, located in exon 3. For intron sequences, we used BLAT [42] to align the *NCYM* mRNA sequence (NR_026766) to the genome of each species and extracted the unmapped regions in the alignment. We found exactly two unmapped regions for each species except for mouse (and thus did not use the mouse sequence). For intergenic regions, we used multiz [43] alignment across 48 species in the browser and cut out 1000-bp sequences that corresponded to human intergenic regions. The sequences of common ancestors were estimated based on the maximum parsimony principle that led to the minimum number of nucleotide-base changes along the already-known phylogenetic tree of the five primates and mice [16]. For multiple possibilities with the same minimum number, we broke the tie by selecting the nucleotide base of the closest outgroup (*e.g.*, when we had A for human, T for chimpanzee, and T for orangutan, we chose T for the common ancestor of human and chimpanzee). When multiple possibilities still remained (as in common ancestor 1), we considered all the possibilities to be equally probable. We estimated common ancestor sequences only within close species (human, chimpanzee, orangutan, and rhesus macaque). We used BLAST [44] to make an alignment between two translated amino-acid sequences ending at the first terminal codon, and calculated K_a and K_s using the KaKs_Calculator [45] with the 'gMYN' method, where K_a and K_s are the rates of non-synonymous and synonymous amino-acid changes, respectively. All pairs of sequences were aligned entirely from the start codon to the terminal codon and did not include any indels, except for the alignment between common ancestor 2 and common ancestor 3, for which we noted 'frameshift' instead of the K_a and K_s values.

We measured a bias in the codon frequencies (or amino acid frequencies) through the deviation from the uniform usage of each codon, using the Chi-squared statistic normalized to the number of codons:

$$\text{Bias} = \left(\sum_{i=1}^{k} \frac{\left(n_i - \frac{N}{k}\right)^2}{\frac{N}{k}} \right) / k,$$

where n_1, …, n_k ($n_i \neq 0$) are the observed number of codon 1, …, and that of codon k, respectively. N is $n_1+\ldots+n_k$. We used R for the calculations and computed the P-values using a Monte-Carlo simulation with 10,000 replicates.

Generation of a human NCYM antibody

A polyclonal anti-NCYM antibody was raised in rabbits against a 14-amino acid stretch at the C-terminal region of NCYM (84-LGTRPLDVSSFKLK-97) (Medical and Biological Laboratories, Nagoya, Japan). The specificity of the purified antibody's affinity was assessed by immunoblotting.

Immunohistochemistry

Neuroblastoma tissues obtained from mice were fixed in 4% paraformaldehyde and paraffin-embedded for histological studies. Tissue sections were stained with hematoxylin and eosin (H&E) and examined histologically by pathologists for confirmation of the tumor type. Tissue arrays (FDA808a-1 and FDA808a-2, US Biomax, Rockville, MD, USA) were used for the analyses of NCYM or MYCN expression in normal and tumorous human tissues. For immunohistochemistry, tissue sections were stained with the polyclonal anti-NCYM antibody we generated, an anti-MYCN antibody (Calbiochem, San Diego, CA, USA), and cleaved Caspase-3 (Cell Signaling Technology).

Immunofluorescence

MYCN-amplified human neuroblastoma TGW cells grown on coverslips were fixed with 4% paraformaldehyde in 1× PBS for 20 min at 4°C, permeabilized with 0.1% Triton-X for 20 min at room temperature, and then incubated with 2% BSA and 3% goat serum in PBS for 1 h to reduce nonspecific binding. Immunostaining was performed by incubating cells with the polyclonal anti-NCYM antibody and a monoclonal anti-MYCN antibody (Calbiochem) for 2 h at room temperature in a humidified chamber, followed by incubation with fluorescent-conjugated goat anti-rabbit IgG (diluted 1:400) or fluorescent-conjugated goat anti-mouse IgG (diluted 1:400), respectively. The coverslips were washed extensively with PBS, mounted in VECTASHIELD mounting medium with DAPI (Vector Laboratories, Burlingame, CA, USA) and images were captured using a confocal microscope (DMI 4000B, Leica).

Plasmids

We previously made a MYCN-luc (+1312) plasmid that contains the region of MYCN promoter region spanning from −221 to +1312 (where +1 represents the transcription start site) [27]. Luciferase reporter plasmids containing different lengths of

the MYCN promoter were generated from MYCN-Luc (+1312) by partial removals of the *MYCN* promoter region with appropriate restriction enzymes. The MYCN promoter region in MYCN-luc (+1312) was subcloned into the pGL3basic vector or pGL4.17Δ*Eco*RV *Eco*RI vector in the opposite direction for generation of NCYM-luc vectors. pGL4.17 Δ*Eco*RV *Eco*RI was the luciferase reporter plasmid, where an *Eco*RV site in pGL4.17 (Promega, Southampton, UK) is replaced with an *Eco*RI site. NCYM-luc E-box WT and NCYM-luc E-box MT were generated by PCR-based amplification using MYCN-luc (+1312) as a template. Oligonucleotide primers used were as follows: 5′-AACCAGGTTCCCCAATCTTC-3′ (forward) and 5′-ACCACCCCCTGCATCTGCAT-3′ (reverse, NCYM-luc E-box WT) or 5′-ACCACCCCCTGCATCCGCAT-3′ (reverse, NCYM-luc E-box MT). Underlined sequences in the reverse primers indicate the wild-type or mutant E-boxes. The NCYM complementary DNA was introduced into a pcDNA3 expression vector, comprising a FLAG-tag at the 5′ locus of NCYM to generate pcDNA3-FLAG-*NCYM*. The sequence of the entire *NCYM* open reading frame was confirmed by sequencing. The FLAG-*NCYM* cDNA was ligated downstream of the rat *TH* promoter in the pGEM7z(f+) expression plasmid, which was originally made from a *MYCN* transgenic construct [21] by excision of the *MYCN* gene, to generate pGEM7z(f+)-FLAG-*NCYM*.

Cell culture, infection, transfection, and RNA interference

Human neuroblastoma cell lines SH-SY5Y, SK-N-AS, NLF, IMR32, CHP134, and SK-N-BE were maintained in RPMI-1640 medium supplemented with 10% fetal bovine serum (FBS) and antibiotics. Human neuroblastoma cell line BE (2)-C was maintained in a 1:1 mixture of minimal essential medium (MEM, Gibco by Life technologies, Carlsbad, CA, USA) and Ham's Nutrient Mixture F12 (Gibco) supplemented with 15% heat inactivated fetal bovine serum (FBS) (Gibco) with MEM non-essential amino acids (Gibco) and antibiotics. Mouse neuroblastoma cell line Neuro 2a was maintained in DMEM supplemented with 10% FBS and antibiotics. NLF, IMR32, CHP134, SK-N-BE, and BE (2)-C have amplified *MYCN*, whereas SH-SY5Y, SK-N-AS, and Neuro 2a are cell lines with a single copy of *MYCN*. The cells or tissues with a single copy of *MYCN* have one copy of *MYCN* gene in a haploid genome. Lentivirus was produced by co-transfecting cDNA or shRNA expression plasmids with pCMVR and pMDG plasmids into HEK293T cells using FuGENE HD reagent (Roche, Mannheim, Germany). The MYCN and NCYM shRNA expression plasmids contained pLKO.1-puro as the backbone (Sigma, St Louis, MO, USA). At 24 and 48 h after transfection, the viral supernatants were collected and mixed with neuroblastoma cells. Other plasmid transfections were done using Lipofectamine 2000 transfection reagent (Invitrogen, Karlsruhe, Germany) according to the manufacturer's instructions. The target sequences of the shRNAs used were as follows: NCYM sh-1 (N-cym1 custom shRNA, Sigma) 5′-tggcaattgcttgtcattaaa-3′, NCYM sh-2 (N-cym 2 custom shRNA, Sigma) 5′-gaggttgctcctgtgtaatta-3′, NCYM sh-3 (N-cym 3 custom shRNA, Sigma) 5′-tcctgtgtaattacgaaagaa-3′, MYCN sh-1 (TRCN0000020694, Sigma) 5′-gccagtattagactggaagtt-3′, MYCN sh-2 (TRCN0000020695, Sigma) 5′-cagcagcagttgctaaagaaa-3′. The control shRNA (SHC002) was purchased from Sigma.

RNA isolation, RT-PCR and quantitative real-time RT-PCR

Total RNA was isolated from the frozen tumor samples and adrenal tissues of transgenic mice with ISOGEN (NIPPON GENE, Tokyo, Japan), and treated with RNase-free DNase I. Total RNA from neuroblastoma cells (CHP134 and SK-N-AS) was prepared using an RNeasy Mini kit (Qiagen, Valencia, CA) following the manufacturer's instruction. cDNA was synthesized using SuperScript II with random primers (Invitrogen). Quantitative real-time RT-PCR (qRT-PCR) using an ABI PRISM 7500 System (Applied Biosystems, Foster City, CA) was carried out using a SYBR green PCR reaction. The primer sets used were as follows: (for clinical experiments using primary neuroblastomas) human *MYCN*, 5′-ggacaccctgagcgattcag-3′, and 5′-aggaggaacgccgcttct-3′, human *NCYM* 5′-ccgacagctcaaacacagaca-3′ and 5′- gtaatggcttctgcgaaaagaaa-3′; (for cellular experiments) human *MYCN*, 5′-tccatgacagcgctaaacgtt-3′ and 5′- ggaacacacaaaggtgacttcaaca-3′, human *NCYM*, 5′-cgcccccttaggaacaagac-3′ and 5′- gcgcccctcttctttcaatt-3′, mouse *MYCN*, 5′-tcgggacactaaggagcttca-3′ and 5′-ggaatcttggaccggaacaa-3′, mouse *GAPDH*, 5′-gggaagcccatcaccatct-3′ and 5′-cggcctcaccccatttg-3′. The mRNA levels of each of the genes were standardized by *β-actin* or *GAPDH*.

Luciferase assay

SK-N-AS cells were co-transfected with the indicated reporter constructs and the pRL-TK *Renilla* luciferase cDNA together with increasing amounts of the expression plasmid for MYCN or MYC. Total DNA per transfection was kept constant (510 ng) by adding pcDNA3 (Invitrogen). Forty-eight hours after transfection, firefly and *Renilla* luciferase activities were measured with a dual-luciferase reporter assay system according to the manufacturer's instructions (Promega).

Immunoblotting

We resolved cell proteins by SDS-PAGE before electro-blotting onto PVDF membranes. We incubated the membranes with the following primary antibodies overnight: anti-NCYM (1:1000 dilution), anti-MYCN antibody (1:1000 dilution; Calbiochem and Cell Signaling), anti-Lamin B (1:1000 dilution; Calbiochem), anti-α-tubulin (1:1000 dilution; Santa Cruz, CA, USA), anti-GST (1:1000; Santa Cruz), anti-GSK3β (1:1000 dilution; Cell Signaling), anti-phospho-GSK3β (S9) (1:1000 dilution; Cell Signaling), anti-β-catenin (1:1000 dilution; Cell Signaling), anti-phospho-AKT (S473) (1:1000 dilution; Cell Signaling), anti-phospho-AKT (S308) (1:1000 dilution; Cell Signaling), anti-AKT (1:1000 dilution; Cell Signaling), anti-S6K (1:1000 dilution; Cell Signaling), anti-phospho-S6K (T389) (1:1000 dilution; Cell Signaling), and anti-actin (1:4000 dilution; Sigma). The membranes were then incubated with a horseradish peroxidase-conjugated secondary antibody (anti-rabbit IgG at 1:2000–1:4000 dilution or anti-mouse IgG at 1:2000 dilution; both from Cell Signaling Technology) and the bound proteins were visualized using a chemiluminescence-based detection kit (ECL and ECL pro kit, Amersham, Piscataway, NJ, USA; ImmunoStar LD, Wako).

Immunoprecipitation

Whole lysates prepared from CHP134 cells or tumor tissues were pre-cleared by incubation with protein G-Sepharose beads (Amersham Pharmacia Biotech) for 1 h at 4°C. The supernatant was collected after a brief centrifugation, and incubated with the indicated primary antibodies at 4°C overnight. The immune complexes were precipitated with protein G-Sepharose beads for 1 h at 4°C, and the non-specific bound proteins were removed by washing the beads with lysis buffer five times at 4°C. Different lysis buffers were used for the cell-based experiments (50 mM Tris-HCl pH 8.0, 137 mM NaCl, 2.7 mM KCl, and 1% Triton X) and for the tumor tissues (50 mM Tris-HCl pH 8.0, 1 mM EDTA, 0.2% DOC and 0.2% SDS). The immunoprecipitated proteins were eluted by boiling in Laemmli sample buffer and analyzed by immunoblotting.

Analysis of MYCN stability

CHP134 cells were cultured with 50% lentiviral supernatant for transfection of the indicated shRNA. Forty-eight hours after the transfection, cycloheximide (Sigma) was added to the culture medium at a final concentration of 50 μg/ml and cells were harvested at the indicated time points. For MG132 treatment, 44 h after the transfection, cells were treated with DMSO or 10 μM MG132 for 4 h.

Purification of NCYM protein from bacteria

DH5α cells were transformed with pGEX-4T-*NCYM* plasmid and cultured in Luria Broth (LB) at 37°C. The expression of the GST-NCYM fusion protein was induced by culturing the cells with 1 mM IPTG for 10 h at 25°C. Cells were collected by centrifugation, dissolved in cell lysis buffer (PBS, 1% TritonX-100, 5 mM EDTA and protease inhibitors), and stored at −80°C. Cell extracts were obtained by thawing the frozen cells, followed by sonication and ultra-centrifugation. After a pulldown with glutathione sepharose 4B beads, the beads were washed five times in cell lysis buffer and once in thrombin buffer containing 50 mM Tris-HCl pH 8.0, 150 mM NaCl, 2.5 mM $CaCl_2$, 5 mM $MgCl_2$, 1 mM DTT. GST-Tag cleavage mediated by thrombin released the full-length NCYM protein from the beads and the thrombin was removed by adding p-aminobenzamidine agarose beads according to the standard protocol. The full length NCYM protein was further purified by filtration using Amicon Ultra-4 (Millipore, Temecula, CA, USA), and dissolved in stock buffer (50 mM Tris-HCl pH 8.0, 150 mM NaCl, 5 mM EDTA, 0.25 mM DTT, 10% sodium azide, 50% glycerol and protease inhibitors) and stored at −20°C. Complete PIC (Roche) was used for protease inhibition.

GST-pulldown assay

For GST-pulldown assay, 0.5 μg of purified NCYM proteins were incubated with 0.5 μg of GST protein or GST-fused CDK1/Cyclin B1 (Signal Chem, Richmond, Canada), GSK3β (Promega) and MYCN (Abnova, Taipei, Taiwan) for 2 h at 4°C. Bound complexes were recovered on the glutathione-sepharose beads, washed with the binding buffer (50 mM Tris-HCl, pH 8.0, 1 mM EDTA, 150 mM NaCl, 0.1% Nonidet P-40 and Complete PIC), boiled in in Laemmli sample buffer and analyzed by immunoblotting.

In vitro kinase assay

For MYCN phosphorylation, two kinase reactions were performed sequentially. The first kinase reactions were performed for 1 h in kinase buffer (40 mM Tris-HCl pH 7.5, 20 mM $MgCl_2$, 0.1 mg/ml BSA, 50 μM DTT) in the presence of 50 μM Ultrapure ATP (Promega), 50 ng of purified MYCN (Abnova), and 40 ng of purified CDK1/Cyclin B1 (Signal Chem) at room temperature. At 1 h, the first reaction solution was mixed with the same volume of kinase buffer containing 100 nM CDK1 inhibitor (CGP74514A, Calbiochem), 4 μCi of [γ-^{32}P] ATP (PerkinElmer), and 20 ng of purified GSK3β with the indicated amounts of purified NCYM or purified GST. The second reaction was performed for 1 h at room temperature. The amount of phosphorylated MYCN was quantified using standard autoradiography. The total amount of MYCN was quantified by using an Oriole Fluorescent Gel stain (Bio-Rad). We also examined whether purified NCYM could be a substrate of GSK3β using the ADP-Glo system (Promega) according to manufacturer's instructions. Reactions were performed for 1 h in kinase buffer (40 mM Tris-HCl pH 7.5, 20 mM $MgCl_2$, 0.1 mg/ml BSA, 50 μM DDT) in the presence of 25 μM Ultrapure ATP (Promega) and 25 ng of purified GSK3β with increasing amounts of NCYM or GST at room temperature. The peptide of human muscle glycogen synthase-1 (YRRAAVPPSPSLSRHSSPHQ(pS)EDEEE) was used as a positive control for the GSK3β substrate. At 1 h, the reaction solutions were mixed and incubated with ADP-Glo reagent for 40 min at room temperature, and the mixture was combined with a kinase detection reagent and allowed to stand for 30 min. The kinase activities were detected using a luminometer (PerkinElmer ARVOX3).

TUNEL staining

The indicated neuroblastoma cells were transfected with the indicated shRNA with 50% lentiviral supernatant. Seventy-two hours after transfection, all cells were collected by centrifugation, attached onto the coverslips by CYTOSPIN 4 (Thermo Fisher Scientific, Wilmington, DE, USA), and fixed in 4% paraformaldehyde for 1 h. Apoptotic cells were detected by using an *in situ* cell death detection kit (Roche) according to the manufacturer's protocol. The coverslips were mounted with DAPI-containing mounting medium (Vector Laboratories) and observed under a confocal microscope.

Cell viability assay (MTT assay)

Cell viability was quantified by the 3-(4, 5-dimethylthiazol-2-yl)-2, 5-diphenyltetrazolium bromide (MTT) method. Cells were collected and seeded in 96-well plates at 1×10^4 cells/ml. After addition of 10 μl of MTT tetrazolium salt (Sigma) solution to each well, the plates were incubated in a CO_2 incubator for 60 min. The absorbance of each well was measured using a Dynatech MR5000 plate reader with a test wavelength of 450 nm and a reference wavelength of 630 nm.

Migration and invasion assay

The invasive potential of BE (2)-C cells *in vitro* was measured by evaluating the number of invading cells using Matrigel-coated trans-well inserts (BD Biosciences) according to the manufacturer's instructions. BE (2)-C cells transfected with the indicated shRNA were seeded onto an insert containing 8 μm pores (BD Biosciences) in a 24-well plate at 1×10^5 cells/ml. Cells on the lower side of the membrane were fixed with 4% paraformaldehyde and stained using a Diff Quick Staining Kit (Sysmex).

Generation of transgenic mice

All animal experimental procedures used in this study were reviewed and approved by the Committee on the Ethics of Animal Experiments of the Chiba Cancer Center (Permit Number: 12-13). Linearized and purified pGEM7z (f+)-FLAG-*NCYM* was injected into the pronuclei of fertilized eggs derived from 129/SvJ×C57BL/6J mice. We selected four lines of *NCYM* transgenic mice according to the level of *NCYM* expression in adrenal tissues (Figure S15B), and the transgenic mice were backcrossed to 129/SvJ at least 10 times to generate *NCYM* transgenic mice. To generate *MYCN/NCYM* double transgenic mice, the *NCYM* transgenic mice were crossed with *MYCN* transgenic mice of the 129/SvJ strain. On the basis of breeding schemas, all mice carrying the *MYCN* transgene were hemizygous. Tail DNA was analyzed for *MYCN* and *NCYM* transgenes, and the *NCYM* transgene copy number was quantified by quantitative genomic PCR. The primer sets used for genotyping were as follows: *NCYM*, 5′-cgcccccttaggaacaagac-3′ and 5′- gcgcccctcttctttcaatt-3′, *MYCN*, 5′-tggaaagcttcttattggtagaaacaa-3′ and 5′-agggatcctttccgccccgttcg-tttaa-3′.

Detection of metastatic tumors in mice

If more than one tumor over 2 mm in a diameter separately developed in a different organ, we defined this as the mouse having macroscopic metastatic tumors. In Figure 4C, only the number of mice with macroscopic metastatic tumors was counted. As a preliminary experiment, we used microscopy to detect tumors in the brain, pancreas, spleen, heart, lungs, kidneys and liver in nine mice (*MYCN/NCYM* double transgenic mice; n = 6, *MYCN* transgenic mice; n = 3). In addition to macroscopic metastases in the brain, heart, ovary and uterus, we found microscopic metastases in the lungs of *MYCN/NCYM* double transgenic mice, but the mass of these tumor cells was not large enough to be visible by eye. We also microscopically analyzed the HE-stained bone marrow from the hind legs of 19 mice (*MYCN/NCYM* double transgenic mice, n = 10; *MYCN* transgenic mice, n = 9). However, no metastatic tumor cells were found in the bone marrow.

Murine therapy

All mice were genotyped to detect the presence of human *MYCN* or *NCYM* transgenes. After weaning, at about 30 days old, *MYCN* transgenic mice or *MYCN/NCYM* double transgenic mice were palpated for intra-abdominal tumors every day. Mice of either genotype found with palpable tumors were treated with NVP-BEZ235 (Cayman Chemical, Ann Arbor, MI, USA) (35 mg/kg in PEG300) or vehicle (PEG300, Wako) once daily for 30 days by oral gavage. All mice were monitored until euthanasia was required in accordance with the institutional animal committee.

Tumor specimens

The 106 human neuroblastoma specimens used in the present study were kindly provided by various institutions and hospitals in Japan to the Chiba Cancer Center Neuroblastoma Tissue Bank. Written informed consent was obtained at each institution or hospital. This study was approved by the Chiba Cancer Center Institutional Review Board. Tumors were classified according to the International Neuroblastoma Staging System (INSS): 27 Stage 1, 15 Stage 2, 34 Stage 3, 23 Stage 4, and 7 Stage 4 s. Clinical information including age at diagnosis, tumor origin, Shimada's histology, prognosis and survival duration of each patient was obtained. The patients were treated following the protocols proposed by the Japanese Infantile Neuroblastoma Cooperative Study and the Group for the Treatment of Advanced Neuroblastoma and subjected to survival analysis. Cytogenetic and molecular biological analysis of all tumors was also performed by assessing DNA ploidy, *MYCN* amplification and *TrkA* expression, as previously described [46].

Array CGH analysis

Array CGH analysis was conducted using the Human Genome CGH 244K Oligo Microarray Kit (G4411B, Agilent Technologies, Santa Clara, CA, USA). Genomic DNA prepared from primary neuroblastoma tissues or cell lines was labeled with Cy3-dye using a QuickAmp labeling kit. Human placental DNA was labeled with Cy5-dye and used as a reference control. Labeling, hybridization and subsequent data processing by FeatureExtraction and CGH-Analytics software were performed according to the manufacturer's instructions. Relative copy number of the probes surrounding the *MYCN* and *NCYM* genomic locus (from *DDX1* to *FAM49A*) were compared in each primary tumor or cell line.

Statistical analysis

Statistical significance was tested as follows: two-group comparison of survival by log-rank test, correlation of gene expression by Pearson's correlation coefficient test or Student's *t*-test, multivariate analysis for survival by Cox regression model, and the rate of mouse genotype and metastatic tumor occurrence in line 6 was calculated by Chi-square independence test and Mann–Whitney U test, respectively.

Supporting Information

Figure S1 Alignment of NCYM coding sequences. Primate sequences were extracted from the UCSC genome browser on the basis of conservation, and common-ancestor sequences were estimated based on the maximum parsimony principle. Nucleotide changes are colored in orange. Post-terminal sequences are colored in blue. Post-terminal sequence refers to the DNA sequence after the first terminal codon up to the position corresponding to the first terminal codon in the human sequence. CA indicates common ancestor.
(TIF)

Figure S2 Analysis of the bias of codon (and amino acid) usage and evolutionary rates in the *NCYM* gene. (A) Distribution of NCYM protein length, numbers of end codons, and the bias of codon and amino acid usage. Asterisk indicates statistical significance ($P<0.001$, Monte-Carlo Chi-square test). Graph showing the number of codons (B) or amino acids (C) in the NCYM protein of different species.
(TIF)

Figure S3 Exogenous NCYM protein can be expressed in cells. (A) Purification of NCYM protein from bacteria. GST fusion NCYM was overexpressed in bacterial cells and purified by GST-pulldown. The GST-NCYM protein was further cleaved by thrombin, and full-length NCYM was purified. The left panel shows CBB staining and the right panel shows a western blot using anti-NCYM antibody. The arrow indicates the NCYM protein; the asterisk indicates the degraded NCYM protein. (B) Human NCYM protein expression in mouse neuroblastoma Neuro 2a cells. Neuro 2a cells were transfected with increasing amounts of NCYM expression plasmid (1, 1.5, 2 μg) for 48 h. The cell lysates were subjected to western blotting to verify the expression of human NCYM using an anti-NCYM antibody. The arrow indicates the NCYM protein; the asterisk indicates a non-specific band.
(TIF)

Figure S4 Subcellular localization of NCYM protein in neuroblastoma cells. (A) Localization of NCYM protein in neuroblastoma cells. The indicated neuroblastoma cells were biochemically fractionated into nuclear and cytoplasmic fractions followed by immunoblotting with anti-NCYM antibody. Lamin B and α-tubulin were used as nuclear and cytoplasmic markers, respectively. SK-N-AS and SH-SY5Y are human neuroblastoma cells with a single copy of *MYCN*, and NLF, IMR32, CHP134, and SK-N-BE are human neuroblastoma cells with amplified *MYCN*. (B) Nuclear staining of NCYM and MYCN protein in *MYCN*-amplified human neuroblastoma TGW cells analyzed by confocal fluorescence microscopy. Scale bar, 50 μm.
(TIF)

Figure S5 NCYM protein expression in human normal and neuroblastoma tissues analyzed by immunohistochemistry. The indicated human normal tissues (tissue array, FDA808a-1) were stained with anti-NCYM antibody. (A) Cerebellum; scale bar, 100 μm. (B) Testis; scale bar, 50 μm. (C) Pancreas; scale bar, 100 μm. (D) Heart; scale bar, 100 μm. (E) Human metastatic neuroblastoma in the liver (Stage 4S); scale bar, 50 μm. (F) Human

metastatic neuroblastoma in the lymph node (Stage 4); scale bar, 50 μm.
(TIF)

Figure S6 Expression of NCYM and MYCN protein in human thyroid tumors analyzed by immunohistochemistry. Normal and cancerous human tissues (tissue array, FDA808a-2) were stained with anti-NCYM (A and B) or anti-MYCN antibody (C and D). (A), (C), Normal thyroid. (B), (D), Thyroid tumors. Scale bars, 100 μm.
(TIF)

Figure S7 Co-amplification of *MYCN* and *NCYM* genes in human neuroblastoma cell lines and primary neuroblastomas. Average gene copy number was calculated based on the signals of multiple probes targeted to the indicated gene in array CGH. Twenty-three *MYCN*-amplified human neuroblastoma cell lines (A) or 23 human primary neuroblastomas (B) were analyzed by array CGH.
(TIF)

Figure S8 High *NCYM* mRNA expression is associated with poor prognosis in neuroblastomas without *MYCN* amplification. *MYCN* non-amplified neuroblastomas diagnosed at over one year of age were analyzed using Kaplan–Meier survival curves based on the expression levels of *NCYM* mRNA (A) or *MYCN* mRNA (B). The expression levels of *NCYM* or *MYCN* mRNA were examined by qRT-PCR and normalized by *GAPDH*. The average of the expression levels was used as a threshold to divide the tumors with low expression (open circle; A, n = 36, B, n = 34) from those with high expression (closed circle; A, n = 9, B, n = 11). *P* values of (A) and (B) were 0.0375 and 0.144, respectively (Log-rank test).
(TIF)

Figure S9 MYCN, but not MYC, activates *MYCN* transcription in human neuroblastoma cells. (A) Schematic drawing of the *MYCN/NCYM* promoter region. (B) Relative mRNA levels of *MYC*, *MYCN* and *NCYM* in SK-N-AS *MYCN* single copy human neuroblastoma cells transfected with 2 μg of a MYC expression vector. mRNA levels were measured by qRT-PCR with *β-actin* as an internal control. (C) Luciferase reporter assays. SK-N-AS cells were transiently co-transfected with a constant amount of the indicated luciferase reporter constructs bearing various lengths of the human *MYCN* promoter region (100 ng), a *Renilla* luciferase reporter plasmid (pRL-TK) (10 ng), and either an empty plasmid (pcDNA3) or with an increasing amount (200, 300, 400 ng) of the expression plasmid for MYCN. Forty-eight hours after transfection, cells were lysed and their luciferase activities were measured.
(TIF)

Figure S10 An intact upstream E-box is required for the activation of the NCYM promoter by MYCN. (A) The NCYM promoter sequence. The sequences of primer sets used in our previous report [27] are shown as MYCN ChIP Forward (Reverse) Primer. The recruitment of the MYCN protein to its own intron 1 was detected using those primers. The putative E-box sequence is indicated in red characters. (B) MYCN, but not MYC, enhances NCYM promoter activity. Human neuroblastoma SK-N-AS cells were transfected with 400 ng of the MYCN expression plasmid for 48 hours and then their luciferase activity was measured. (C) The effect of an E-box mutation on MYCN-induced NCYM promoter activity. The WT and mutant NCYM promoters were evaluated for transcriptional activity 24 hours after the transfection of the expression plasmids for MYCN or MYC. The asterisks indicate statistical significance ($P<0.01$, Student's *t*-test).
(TIF)

Figure S11 NCYM stabilizes the MYCN protein in the ubiquitin proteasome system dependent manner. (A) Western blot analysis and RT-PCR. Both NCYM and its SNP type (NCYML70V) induce MYCN expression levels in CHP134 cells. (B) Western blot analysis of MYCN expression in CHP134 cells transfected with NCYM or control shRNA, followed by treatment with 50 μM cycloheximide (CHX), and harvested at the indicated time points. (C) Proteasome inhibitor MG132 treatment of NCYM knockdown CHP134 cells. Western blot analysis showed that NCYM-mediated downregulation of MYCN is inhibited by MG132 treatment. Actin was used as a loading control.
(TIF)

Figure S12 GSK3β does not phosphorylate NCYM protein. (A) *In vitro* kinase assay. The phosphorylation of the control substrate human glucose synthase 1 by GSK3β was measured to test the assay system. (B) The correlation between the percentage of ADP and the relative kinase activity measured by luciferase activity ($R^2 = 0.9994$). (C) The relative kinase activity of GSK3β was not increased when GST or NCYM were used as a substrate.
(TIF)

Figure S13 NCYM knockdown promotes apoptosis in *MYCN*-amplified neuroblastoma cells. (A) The relative mRNA levels of *MYCN*, *NCYM* and *MYC* in human neuroblastoma cells. Levels of mRNA were measured by qRT-PCR with *β-actin* as an internal control. (B and C) TUNEL staining. The indicated human neuroblastoma cells were lentivirally transfected with the indicated shRNA. Seventy-two hours after the transfection, cells were fixed in 4% paraformaldehyde and subjected to TUNEL staining. Cell nuclei were stained with DAPI (upper panels). Scale bars, 50 μm. The percentage of TUNEL-positive cells was calculated as the average of three different microscopic fields. SH-SY5Y and SK-N-AS are *MYCN* single copy cells (B), and BE (2)-C and CHP134 are *MYCN*-amplified cells (C).
(TIF)

Figure S14 NCYM knockdown inhibits the proliferation and invasion in BE (2)-C cells. (A) Western blot analysis showed that NCYM knockdown decreased MYCN protein in BE (2)-C cells. (B) Cell proliferation assay. After transfection with NCYM shRNA (closed circle) or control shRNA (open circle), cell proliferation was examined in an MTT assay, at the indicated time points. (C, D) the effect of NCYM knockdown on cellular migration (C) and invasion (D). Three days after the introduction of NCYM shRNA, the cells were adjusted to 1×10^5 cells/ml and subjected to a Boyden chamber invasion assay.
(TIF)

Figure S15 Generation of *MYCN/NCYM* transgenic mice. (A) A *NCYM* cDNA was ligated 3′ to the rat *TH* promoter to generate the pGEM7z(f+)-FLAG-*NCYM* transgenic constructs. (B) *NCYM* mRNA expression in the adrenal tissues of *NCYM* transgenic mice was measured by qRT-PCR. The expression levels were normalized to mouse *GAPDH*. Red arrows indicate the mouse lines used for further experiments. (C) Table showing the distribution of actual numbers of transgenic mice (line 6) resulting from intercrossing of *MYCN* Tg/+ *NCYM* Tg/+ and *NCYM* Tg/+ and the corresponding theoretical numbers ($P>0.05$, Chi-square independence test). This result indicates that the *NCYM* and *MYCN* transgenes have a marginal effect on the embryonic lethality of mice. (D) Kaplan–Meier survival curves of 83 mice resulting from intercrosses of *MYCN* Tg/+ *NCYM* Tg/+ and *NCYM* Tg/+ (mouse line 6). (E) Kaplan–Meier analysis for tumor incidences in *MYCN* Tg/+ and *MYCN/NCYM* Tg mice (mouse line 6).
(TIF)

Figure S16 Neuroblastoma histology of *MYCN* transgenic mice and *MYCN/NCYM* double transgenic mice. (A) Neuroblastomas arise as primary lesions in a *MYCN/NCYM* double transgenic mouse (i) and *MYCN* transgenic mice (ii). Thoracic paraspinal (T1) and abdominal (T2, T3) tumors. K, kidney. (B) H&E staining of T1 (i), T2 (ii), and T3 (iii).
(TIF)

Figure S17 NCYM inhibits apoptosis in the neuroblastomas of *MYCN/NCYM* double transgenic mice. The number of apoptotic cells in neuroblastomas from *MYCN* transgenic mice (A) and *MYCN/NCYM* double transgenic mice (B) were measured using cleaved capase-3 staining. Scale bar, 50 μm. (C) Quantification of cleaved caspase-3–positive areas in the tumors. The apoptotic cells were calculated by averaging the number of cleaved caspase-3 positive areas counted in 5 randomly selected fields (100 μm^2) per slide using WinROOF software (version 7.0, Mitani Corp.). *P* value was 0.012 (Student's *t*-test).
(TIF)

Figure S18 Schematic model of NCYM function in aggressive human neuroblastomas.
(TIF)

Table S1 Correlation between the expression of *NCYM* or *MYCN* and other prognostic factors.
(DOC)

Table S2 Multiple Cox regression analyses of *NCYM* expression, *MYCN* expression, age, *MYCN* amplification, stage, DNA index, Shimada pathology, *TrkA* expression, and origin.
(DOC)

Table S3 Summary of mice bearing neuroblastomas.
(DOC)

Acknowledgments

We thank I. Kuroita, H. Nakamura, and Y. Nakamura for their technical support in the computational data analyses, A. Sada and N. Kitabayashi for DNA and RNA extractions, R. Murasugi for FISH analyses support, T. Ozaki, T. Kamijo, Y. Yamaguchi, Y. Tatsumi, E. Isogai, and T. Yokochi for comments and advice.

Author Contributions

Conceived and designed the experiments: YS AN. Performed the experiments: YS SMRI JA YK MK YT HK SHo WS MO SHa AT. Analyzed the data: YS MK YT HK SHo MI TS MO SHa AT AN. Contributed reagents/materials/analysis tools: DM MY YN. Wrote the paper: YS AN.

References

1. Jacob F (1977) Evolution and tinkering. Science 196: 1161–1166.
2. Ohno S (1970) Evolution by gene duplication. New York, NY, Springer-Verlag.
3. Tautz D, Domazet-Loso T (2011) The evolutionary origin of orphan genes. Nat Rev Genet 12: 692–702.
4. Kaessmann H (2010) Origins, evolution, and phenotypic impact of new genes. Genome Res 20: 1313–1326.
5. Khalturin K, Hemmrich G, Fraune S, Augustin R, Bosch TC (2009) More than just orphans: are taxonomically-restricted genes important in evolution? Trends Genet 25: 404–413.
6. Carvunis AR, Rolland T, Wapinski I, Calderwood MA, Yildirim MA, et al. (2012) Proto-genes and de novo gene birth. Nature 487: 370–374.
7. Li D, Dong Y, Jiang Y, Jiang H, Cai J, et al. (2010) A de novo originated gene depresses budding yeast mating pathway and is repressed by the protein encoded by its antisense strand. Cell Res 20: 408–420.
8. Begun DJ, Lindfors HA, Thompson ME, Holloway AK (2006) Recently evolved genes identified from Drosophila yakuba and D. erecta accessory gland expressed sequence tags. Genetics 172: 1675–1681.
9. Begun DJ, Lindfors HA, Kern AD, Jones CD (2007) Evidence for de novo evolution of testis-expressed genes in the Drosophila yakuba/Drosophila erecta clade. Genetics 176: 1131–1137.
10. Cai J, Zhao R, Jiang H, Wang W (2008) De novo origination of a new protein-coding gene in Saccharomyces cerevisiae. Genetics 179: 487–496.
11. Chen ST, Cheng HC, Barbash DA, Yang HP (2007) Evolution of hydra, a recently evolved testis-expressed gene with nine alternative first exons in Drosophila melanogaster. PLoS Genet 3: e107.
12. Toll-Riera M, Bosch N, Bellora N, Castelo R, Armengol L, et al. (2009) Origin of primate orphan genes: a comparative genomics approach. Mol Biol Evol 26: 603–612.
13. Knowles DG, McLysaght A (2009) Recent de novo origin of human protein-coding genes. Genome Res 19: 1752–1759.
14. Li CY, Zhang Y, Wang Z, Cao C, Zhang PW, et al. (2010) A human-specific de novo protein-coding gene associated with human brain functions. PLoS Comput Biol 6: e1000734.
15. O'Bleness M, Searles VB, Varki A, Gagneux P, Sikela JM (2012) Evolution of genetic and genomic features unique to the human lineage. Nat Rev Genet 13: 853–866.
16. Wu DD, Irwin DM, Zhang YP (2011) De novo origin of human protein-coding genes. PLoS Genet 7: e1002379.
17. Xie C, Zhang YE, Chen JY, Liu CJ, Zhou WZ, et al. (2012) Hominoid-specific de novo protein-coding genes originating from long non-coding RNAs. PLoS Genet 8: e1002942.
18. Brodeur GM (2003) Neuroblastoma: biological insights into a clinical enigma. Nat Rev Cancer 3: 203–216.
19. Brodeur GM, Seeger RC, Schwab M, Varmus HE, Bishop JM (1984) Amplification of N-myc in untreated human neuroblastomas correlates with advanced disease stage. Science 224: 1121–1124.
20. Schwab M, Varmus HE, Bishop JM, Grzeschik KH, Naylor SL, et al. (1984) Chromosome localization in normal human cells and neuroblastomas of a gene related to c-myc. Nature 308: 288–291.
21. Weiss WA, Aldape K, Mohapatra G, Feuerstein BG, Bishop JM (1997) Targeted expression of MYCN causes neuroblastoma in transgenic mice. EMBO J 16: 2985–2995.
22. Cohn SL, London WB, Huang D, Katzenstein HM, Salwen HR, et al. (2000) MYCN expression is not prognostic of adverse outcome in advanced-stage neuroblastoma with nonamplified MYCN. J Clin Oncol 18: 3604–3613.
23. Nakagawara A, Arima M, Azar CG, Scavarda NJ, Brodeur GM (1992) Inverse relationship between trk expression and N-myc amplification in human neuroblastomas. Cancer Res 52: 1364–1368.
24. Armstrong BC, Krystal GW (1992) Isolation and characterization of complementary DNA for N-cym, a gene encoded by the DNA strand opposite to N-myc. Cell Growth Differ 3: 385–390.
25. Krystal GW, Armstrong BC, Battey JF (1990) N-myc mRNA forms an RNA-RNA duplex with endogenous antisense transcripts. Mol Cell Biol 10: 4180–4191.
26. Jacobs JF, van Bokhoven H, van Leeuwen FN, Hulsbergen-van de Kaa CA, de Vries IJ, et al. (2009) Regulation of MYCN expression in human neuroblastoma cells. BMC Cancer 9: 239.
27. Suenaga Y, Kaneko Y, Matsumoto D, Hossain MS, Ozaki T, et al. (2009) Positive auto-regulation of MYCN in human neuroblastoma. Biochem Biophys Res Commun 390: 21–26.
28. Gustafson WC, Weiss WA (2010) Myc proteins as therapeutic targets. Oncogene 29: 1249–1259.
29. Sjostrom SK, Finn G, Hahn WC, Rowitch DH, Kenney AM (2005) The Cdk1 complex plays a prime role in regulating N-myc phosphorylation and turnover in neural precursors. Dev Cell 9: 327–338.
30. Kang JH, Rychahou PG, Ishola TA, Qiao J, Evers BM, et al. (2006) MYCN silencing induces differentiation and apoptosis in human neuroblastoma cells. Biochem Biophys Res Commun 351:192–197.
31. Zhang HH, Lipovsky AI, Dibble CC, Sahin M, Manning BD (2006) S6K1 regulates GSK3 under conditions of mTOR-dependent feedback inhibition of Akt. Mol Cell 24: 185–197.
32. Chanthery YH, Gustafson WC, Itsara M, Persson A, Hackett CS, et al. (2012) Paracrine signaling through MYCN enhances tumor-vascular interactions in neuroblastoma. Sci Transl Med 4: 115ra113.
33. Schramm A, Köster J, Marschall T, Martin M, Schwermer M, et al. (2013) Next-generation RNA sequencing reveals differential expression of MYCN target genes and suggests the mTOR pathway as a promising therapy target in MYCN-amplified neuroblastoma. Int J Cancer 132:E106–115.
34. Johnsen JI, Segerström L, Orrego A, Elfman L, Henriksson M, et al. (2008) Inhibitors of mammalian target of rapamycin downregulate MYCN protein expression and inhibit neuroblastoma growth in vitro and in vivo. Oncogene 27: 2910–2922.

35. Yu F, Gao W, Yokochi T, Suenaga Y, Ando K, et al. (2013) RUNX3 interacts with MYCN and facilitates protein degradation in neuroblastoma. Oncogene [epub ahead of print]
36. Otto T, Horn S, Brockmann M, Eilers U, Schüttrumpf L, et al. (2009) Stabilization of N-Myc is a critical function of Aurora A in human neuroblastoma. Cancer Cell 15:67–78.
37. Berry T, Luther W, Bhatnagar N, Jamin Y, Poon E, et al. (2012) The ALK(F1174L) mutation potentiates the oncogenic activity of MYCN in neuroblastoma. Cancer Cell 22: 117–130.
38. Heukamp LC, Thor T, Schramm A, De Preter K, Kumps C, et al. (2012) Targeted expression of mutated ALK induces neuroblastoma in transgenic mice. Sci Transl Med 4: 141ra191.
39. Molenaar JJ, Domingo-Fernandez R, Ebus ME, Lindner S, Koster J, et al. (2012) LIN28B induces neuroblastoma and enhances MYCN levels via let-7 suppression. Nat Genet 44: 1199–1206.
40. Valentijn LJ, Koster J, Haneveld F, Aissa RA, van Sluis P, et al. (2012) Functional MYCN signature predicts outcome of neuroblastoma irrespective of MYCN amplification. Proc Natl Acad Sci U S A 109: 19190–19195.
41. Li Z, Tan F, Thiele CJ. (2007) Inactivation of glycogen synthase kinase-3beta contributes to brain-derived neutrophic factor/TrkB-induced resistance to chemotherapy in neuroblastoma cells. Mol Cancer Ther 6:3113–3121.
42. Kent WJ (2002) BLAT–the BLAST-like alignment tool. Genome Res 12: 656–664.
43. Blanchette M, Kent WJ, Riemer C, Elnitski L, Smit AF, et al. (2004) Aligning multiple genomic sequences with the threaded blockset aligner. Genome Res 14: 708–715.
44. Altschul SF, Madden TL, Schaffer AA, Zhang J, Zhang Z, et al. (1997) Gapped BLAST and PSI-BLAST: a new generation of protein database search programs. Nucleic Acids Res 25: 3389–3402.
45. Wang D, Zhang Y, Zhang Z, Zhu J, Yu J (2010) KaKs_Calculator 2.0: a toolkit incorporating gamma-series methods and sliding window strategies. Genomics Proteomics Bioinformatics 8: 77–80.
46. Ohira M, Oba S, Nakamura Y, Isogai E, Kaneko S, et al. (2005) Expression profiling using a tumor-specific cDNA microarray predicts the prognosis of intermediate risk neuroblastomas. Cancer Cell 7: 337–350.

Cancer Medicine

Open Access

ORIGINAL RESEARCH

Identification of novel candidate compounds targeting TrkB to induce apoptosis in neuroblastoma

Yohko Nakamura[1,*], Akiko Suganami[2,*], Mayu Fukuda[1,*], Md. Kamrul Hasan[1], Tomoki Yokochi[1], Atsushi Takatori[1], Shunpei Satoh[1], Tyuji Hoshino[3], Yutaka Tamura[2] & Akira Nakagawara[1]

[1]Division of Biochemistry and Innovative Cancer Therapeutics, Chiba Cancer Center Research Institute, Chiba 260-8717, Japan
[2]Department of Bioinformatics, Graduate School of Medicine, Chiba University, Chiba 260-8670, Japan
[3]Department of Physical Chemistry, Graduate School of Pharmaceutical Sciences, Chiba University, Chiba 260-8675, Japan

Keywords
BDNF, drug discovery, in silico simulations, neuroblastoma, TrkB

Correspondence
Akira Nakagawara, Division of Biochemistry and Innovative Cancer Therapeutics, Chiba Cancer Center Research Institute, Chiba 260-8717, Japan.
Tel: +81-43-264-5431; Fax: +81-43-265-4459; E-mail: akiranak@chiba-cc.jp

Funding Information
This study was supported in part by a Grant-in-Aid from the Ministry of Health, Labour and Welfare for Third Term Comprehensive Control Research for Cancer, JSPS KAKENHI (grant numbers 24249061 and 24592703), and a grant from Takeda Science Foundation.

Received: 20 June 2013; Revised: 31 October 2013; Accepted: 1 November 2013

Cancer Medicine **2014; 3(1): 25–35**

doi: 10.1002/cam4.175

*These authors contributed equally.

Abstract

Neuroblastoma (NB) is one of the most frequent solid tumors in children and its prognosis is still poor. The neurotrophin receptor TrkB and its ligand brain-derived neurotrophic factor (BDNF) are expressed at high levels in high-risk NBs and are involved in defining the poor prognosis of the patients. However, the TrkB targeting therapy has never been realized in the clinic. We performed an in silico screening procedure utilizing an AutoDock/grid computing technology in order to identify novel small chemical compounds targeting the BDNF-binding domain of TrkB. For the first screening, a library of three million synthetic compounds was screened in silico and was ranked according to the Docking energy. The top-ranked 37 compounds were further functionally screened for cytotoxicity by using NB cell lines. We have finally identified seven compounds that kill NB cells with the IC_{50} values of 0.07–4.6 μmol/L. The terminal deoxynucleotidyl transferase dUTP nick end labeling (TUNEL) assay showed that these molecules induce apoptosis accompanied by p53 activation in NB cell lines. The candidate compounds and BDNF demonstrated an antagonistic effect on cell growth, invasion, and colony formation, possibly suggesting competition at the BDNF-binding site of TrkB. The candidate compounds had tumor-suppressive activity in xenograft and in vivo toxicity tests (oral and intravenous administrations) using mice, and did not show any abnormal signs. Using in silico Docking screening we have found new candidate TrkB inhibitors against high-risk NBs, which could lead to new anti-cancer drugs.

Introduction

Neuroblastoma (NB) is one of the most common childhood solid tumors occurring from the precursor cells of the sympathoadrenal lineage of the neural crest cells and is responsible for nearly 8% of all pediatric cancers [1]. The tumors arise in the peripheral nervous system, such as in the adrenal medulla and in sympathetic ganglia. NBs observed within 1 year after birth often regress spontaneously [2–4]. On the other hand, the tumors found in patients over 1 year of age are usually aggressive with poor prognosis, which are frequently associated with chromosomal instability, such as allelic loss of the short arm of chromosome 1, that of the long arm of chromosome 11, gain of chromosome 17q, and amplification of *MYCN* oncogene [5, 6]. In particular, chromosomal deletions at 1p36 and 11q have been detected in many cancers including NB, and thus the genes located in this region have been the candidates as tumor suppressor genes [5–8].

The Trk (NTRK) family of neurotrophin receptors plays a critical role in development and maintenance of the nervous system. This protein family of tyrosine kinase receptors consists of TrkA (NTRK1), TrkB (NTRK2), and TrkC (NTRK3). Activation of Trk family protein receptors

by their preferred neurotrophins (nerve growth factor [NGF] to TrkA, brain-derived neurotrophic factor [BDNF] and NT4/5 to TrkB, and NT3 to TrkC) is closely involved in the survival and differentiation of neurons during development [2–4, 9–13]. TrkB, one of the members of TRK family of tyrosine kinase receptors mentioned above, is involved in regulating neuronal survival and differentiation [2, 4, 11]. We previously reported that the level of TrkA is significantly higher in favorable NB tissues, while TrkB and its ligands, BDNF and NT4/5, are expressed at high levels in unfavorable NBs and function in an autocrine/paracrine manner to promote cell growth and survival [14]. Thus, we hypothesized that a clinical treatment targeting TrkB could improve the prognosis of patients with NB. Toward this end, we performed an in silico screening strategy utilizing grid computing technology (http://www.worldcommunitygrid.org/) to identify novel candidate compounds targeting the BDNF-binding domain of TrkB. The grid-networking system we employed in this project is World Community Gird, which was implemented by the IBM Corporation as a social contribution program. Grid computing technology links many individual computers processing in their spare time, creating a large system with massive computational power far suppressing the power of supercomputers. As the job is split into small pieces that can be processed simultaneously, computation time is reduced from years to days.

In the first screening, a library of synthetic compounds including three million molecules was examined in silico. We further performed in vitro screening assays and identified seven candidate molecules that significantly facilitate growth inhibition in several NB-derived cell lines. We found that these molecules induce apoptosis in NB cell lines at low IC_{50} values, suggesting the molecular mechanism of the cellular growth inhibition. In this study, we demonstrated that novel candidate compounds were rapidly and effectively identified by an in silico Docking screening strategy, followed by in vitro assays. We propose that the candidate compounds targeting the extracellular domain of TrkB could help develop a novel treatment and cure for childhood cancers, including NB.

Material and Methods

In silico screening

The three-dimensional structures of the TrkB/BDNF complex on cell membrane were constructed with MOE (version 2009; CCG Inc., Montreal, Canada) and NAMD (http://www.ks.uiuc.edu/Research/namd/) according to the Brookhaven Protein Databank 1WWB.

The molecular mechanistic calculations were performed to obtain the local minimum structure using Amber99 force field in MOE. In silico screening was performed by using AutoDock (http://autodock.scripps.edu/) and the World Community Grid (http://www.worldcommunitygrid.org/). The three-dimensional structures of these complexes were displayed by using MOE.

Reagents and cell culture

Small molecules were purchased from Namiki Shoji Co. Ltd. (Tokyo, Japan) dissolved in dimethyl sulfoxide (DMSO) at a final concentration of 10 mmol/L, and kept at −20°C. Human NB-derived cell lines were maintained in an RPMI 1640 medium supplemented with 10% heat-inactivated fetal bovine serum at 37°C in a humidified atmosphere of 5% CO_2 in the air.

Proliferation assay

The cells were plated in triplicate at a density of 1×10^4 per well in 24-well culture plates. Twenty-four hours after seeding the cells, the cells were treated with small candidate molecules and DMSO as a control at several concentrations (0.1, 1.0, 10 μmol/L) or left untreated. At the indicated time points after the treatment with the small molecules, cells were trypsinized and the number of viable cells was directly scored using a cell counter. Each experiment was performed in triplicate samples.

TUNEL assay

Cells were grown in a standard culture medium in the presence or absence of the small candidate molecules for indicated periods. Cells were trypsinized, washed with ice-cold phosphate buffered saline (PBS), and then attached to a coverslip using a cytospin centrifuge. Cells were fixed with 4% paraformaldehyde in PBS for 1 h, and permeabilized with 0.1% Triton X-100 and 0.1% sodium citrate in PBS for 2 min. Terminal deoxynucleotidyl transferase dUTP nick end labeling (TUNEL) reaction was performed according to the manufacturer's instructions. The nuclei were stained with DAPI. The coverslips were mounted onto glass slides, and the stained cells were examined by a confocal laser scanning microscope.

Western blotting

Cells growing in the mid-log phase were washed with PBS and a lysis buffer (10% glycerol, 5% 2-mercaptoethanol, 2.3% sodium dodecyl sulfate (SDS), 62.5 mmol/L Tris-HCl, pH 6.8) was added. Whole cell lysate was subjected to SDS/PAGE (polyacrylamide gel electrophoresis) followed by Western blotting.

Cellular assays with BDNF treatment

For colony formation assay, SH-SY5Y cells overexpressing TrkB were treated with the candidate compounds (0, 0.1, and 1 μmol/L) in the absence or presence of BDNF (50 ng/mL) for 2 weeks. Images were taken after crystal violet staining. The number and size of colonies were measured in independent triplicate experiments. For the cell invasion assay, SH-SY5Y cells overexpressing TrkB were treated with the candidate compounds in the absence or presence of BDNF (50 ng/mL) for up to 6 days. Cellular invasion was measured by the Boyden chamber method. For phospho-TrkB assay, SH-SY5Y/TrkB cells were incubated in RPMI 1640 medium without serum for 6 h, then pretreated with the medium in the presence or absence of compound G (100 μmol/L) for 5 min. BDNF in the final concentrations of 0, 5, 15, and 25 ng/mL was added, incubated for 10 min, and then whole cell lysate was prepared. TrkB and phosphorylated TrkB proteins were detected by mouse monoclonal anti-TrkB (Z10) antibody (Santa Cruz Biotechnology, Inc., Dallas, TX) and rabbit polyclonal anti-phospho-TrkB (C50F3) antibody (Cell Signaling Technology, Inc., Danvers, MA), respectively.

Tumor suppression assay utilizing SCID mice

NOD SCID mice (CB-17-Prkdc scid/J) were used for the tumor xenograft experiments. Live animals in this assay were handled, strictly following the protocols and instructions of the Chiba Cancer Center Research Institute, which were approved by our ethics committee. SCID mice were transplanted with CHP134 (5×10^6 cells/100 μL) after 6 weeks of the birth. The compound treatment was initiated at the time when the tumor is about 5 mm^2. The ratio for the injection (amount of compounds/the weight of mouse) was 2 mg per 1 kg. Candidate compounds were dissolved in DMSO and were diluted with a 20% xylitol solution (10-fold dilution). Each mouse was treated with intraperitoneal injection once a day for 14 days. Tumor volume was measured once every 2 days to evaluate the inhibition capability of the candidate drugs. The length and width of each tumor was measured once in every 2 days to evaluate the inhibition capability of the candidate drugs. Tumor volume was calculated according to the following formula: [length × $width^2$]/2 [15, 16]. Animals were treated according to the Institutional Animal Care and Use committee guidelines.

Statistical analysis

The Mann–Whitney test was used to compare differences between two independent groups of the data in Figures 2, 4, and 6. All the statistical analyses were performed by Excel 2002 (Microsoft, Redmond, WA) with statistics add-in module Statcel2 (OMS publishing Inc., Saitama, Japan). A *P*-value of <0.05 was deemed statistically significant.

Results

In silico screening and candidate selection

Our goal was to develop novel drugs to treat and cure the patients with high-risk NB. We performed the in silico Docking simulations using AutoDock software to achieve high-throughput screening. World Community Grid (IBM Corp., Armonk, NY) was utilized to accelerate the computations. Because TrkB, one of the neurotrophin (NT) receptors harboring tyrosine kinase activity, is expressed at high levels in aggressive NB [14], we focused on the extracellular BDNF-binding site of TrkB as the target for the in silico screening. According to the molecular simulation of a ternary structure of the TrkB/NT complex, we determined the amino acid residues that participate in the physical interaction between BDNF and TrkB (Fig. 1) [17]. We set the docking grid to this BDNF-binding domain of TrkB [18] and performed the in silico screening against a library of three million small chemical compounds as potential drug candidates. Using the docked energy scores given by the AutoDock simulations, the molecular profile of the top 100 molecules was

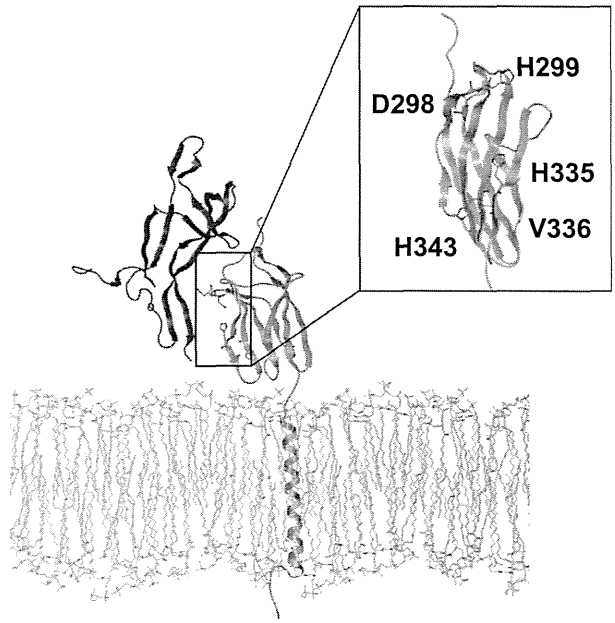

Figure 1. Computational modeling of the specific binding between TrkB (yellow) and BDNF (blue) on the cell membrane (white). 3D structure of TrkB/BDNF on the cell membrane is shown. Inset indicates potential amino acid residues participating in the interaction.

examined in the light of Lipinski's Rule of Five (data not shown) and the highest 60 were chosen for further experiments.

Candidate compounds inhibit the cellular growth in NB cell lines

We expected that the candidate molecules identified above compete with BDNF at the BDNF-binding domain, resulting in inactivation of TrkB activity that triggers the inhibition of the TrkB signaling pathway. As this pathway propagates differentiation and survival signals into the inner part of the cellular fractions, such as the cytosol and the nucleus, endogenous overexpression of the *TrkB* gene frequently found in unfavorable NB may facilitate cellular growth [2, 11, 12, 19, 20]. Therefore, we examined whether the candidate compounds could decrease the growth rate of NB cell lines in which TrkB expression was either detected (CHP134) or overexpressed (SH-SY5Y/TrkB) (Fig. 2A). Among 60 candidates identified using in silico screening, 37 were available for further screening because 23 chemicals could not be obtained or they could not be dissolved in DMSO. CHP134 cells were treated with a fixed concentration of the candidate compounds and finally seven compounds were selected (Table 1), which yielded the highest toxicity. These seven candidate molecules were designated as compounds A–G. In the second screening, CHP134 cells were treated with increasing concentrations of the candidate compounds and then the number of surviving cells were counted 2, 4, and 6 days after the treatment. We confirmed that the candidate compounds decreased the number of surviving cells at the concentrations of either 1 or 10 μmol/L (Fig. 2B). These results suggest that the seven candidate compounds induce cellular growth inhibition in NB cell line. In addition, in the other NB-derived cell line, SH-SY5Y, in which TrkB was stably overexpressed, essentially similar results were obtained (Fig. 2B). To quantify the cell growth inhibition mediated by the candidate compounds, the value of half maximal inhibitory concentration, namely IC_{50}, was evaluated for these seven candidate compounds. In particular, compounds A and G show significantly low IC_{50} values of 0.3 and 0.07 μmol/L, respectively, while the average of IC_{50} values for the seven compounds was 1.9 μmol/L (Table 1). Compounds A and G killed the human foreskin fibroblast cells (strain BJ; ATCC no. CRL2522) at three to five times higher IC_{50} values than NB cell lines (data not shown). On the basis of the chemical structure of compounds A and G (Fig. 3), potential interaction between the compounds and BDNF-binding domain was simulated and this topic is discussed in the Discussion section.

Table 1. IC_{50} values of low-molecular-weight compounds in CHP134 and SH-SY5Y/TrkB cell lines.

Compound	IC_{50} in CHP134 (μmol/L)	IC_{50} in SH-SY5Y/TrkB (μmol/L)
Compound-A	0.29	0.3
Compound-B	1.9	2.0
Compound-C	1.4	2.0
Compound-D	4.6	3.5
Compound-E	2.0	2.2
Compound-F	3.5	3.5
Compound-G	0.07	0.18

Competitive inhibition between candidate compounds and BDNF

To investigate the relationship between the candidate compounds and BDNF, SH-SY5Y/TrkB cells were treated with compounds in the presence or absence of BDNF. Increasing amount of compound A significantly decreased the number of surviving cells, while the cell growth was partially restored in the presence of BDNF under the same treatment with compound A (Fig. 4A, top panels). This result demonstrates that BDNF partially interferes with the cellular toxicity of compound A, suggesting that compound A and BDNF compete to occupy the BDNF-binding domain of TrkB. Similar competitive inhibition by BDNF was observed in the growth inhibitory effect of compound G (Fig. 4A, bottom panels) and five other compounds (data not shown). The colony formation assay showed that the candidate compounds decrease both colony number and colony size even in the presence of BDNF, indicating that the molecules overcome the cell growth activity of BDNF (Fig. 4B). This result suggests that the compounds and BDNF show an antagonistic

Figure 2. Growth inhibitory effects of compounds A–G in neuroblastoma-derived cell lines. (A) Expression levels of TrkB mRNA in SH-SY5Y, SH-SY5Y/TrkB, and CHP134 cells. SH-SY5Y/TrkB is the cells in which TrkB is stably cloned. (B) Growth curves in the presence or absence of compounds A–G. Compounds concentration: open circle (0 μmol/L), filled circle (0.1 μmol/L), filled triangle (1 μmol/L), filled square (10 μmol/L). The cell numbers were represented as the relative values compared to those without the compounds (open circle) at the time of 6 days (set to 1). The *P*-values between the open circle (0 μmol/L) and filled square (10 μmol/L) at day 6 were less than 0.05 in all experiments using seven compounds.

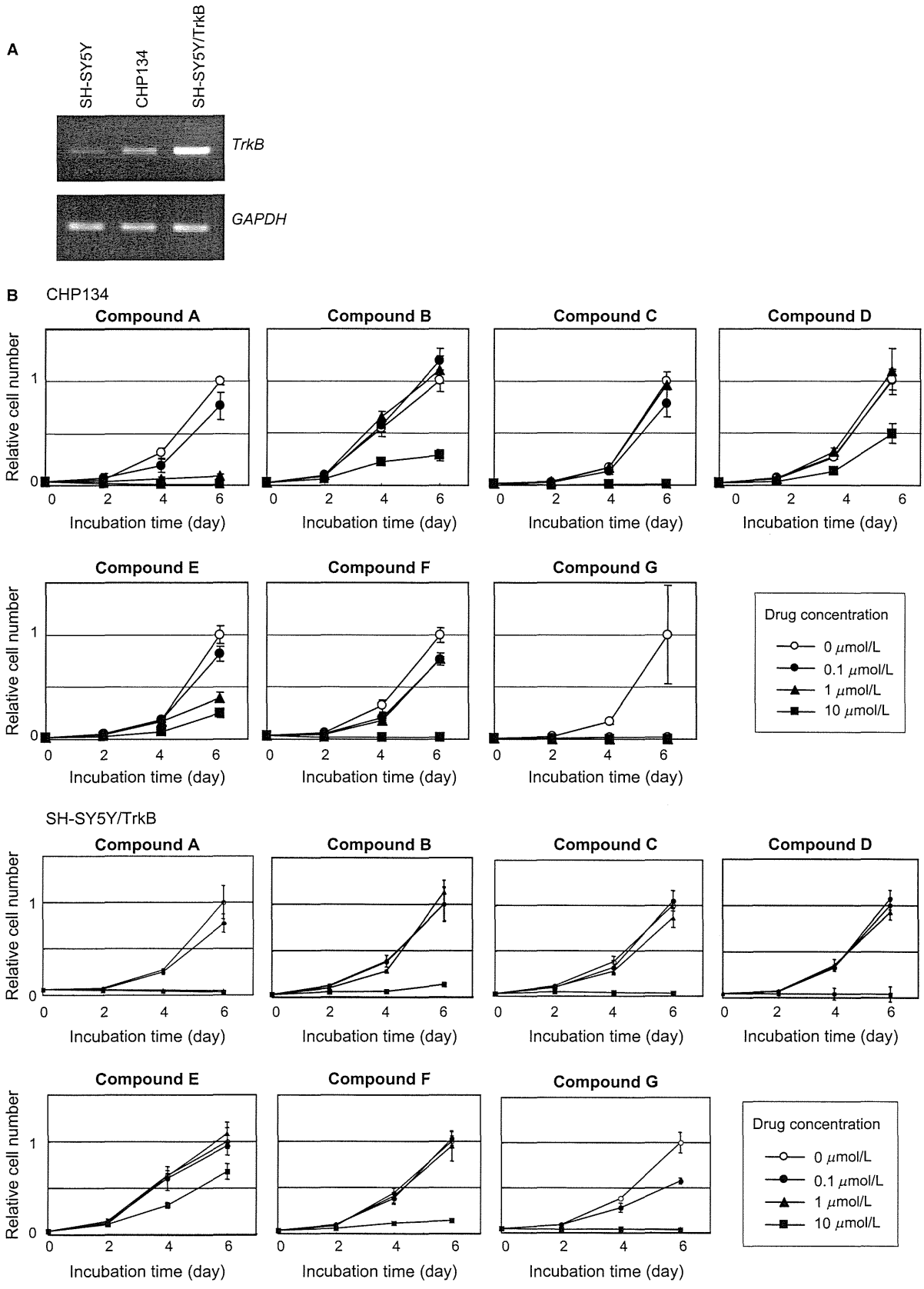

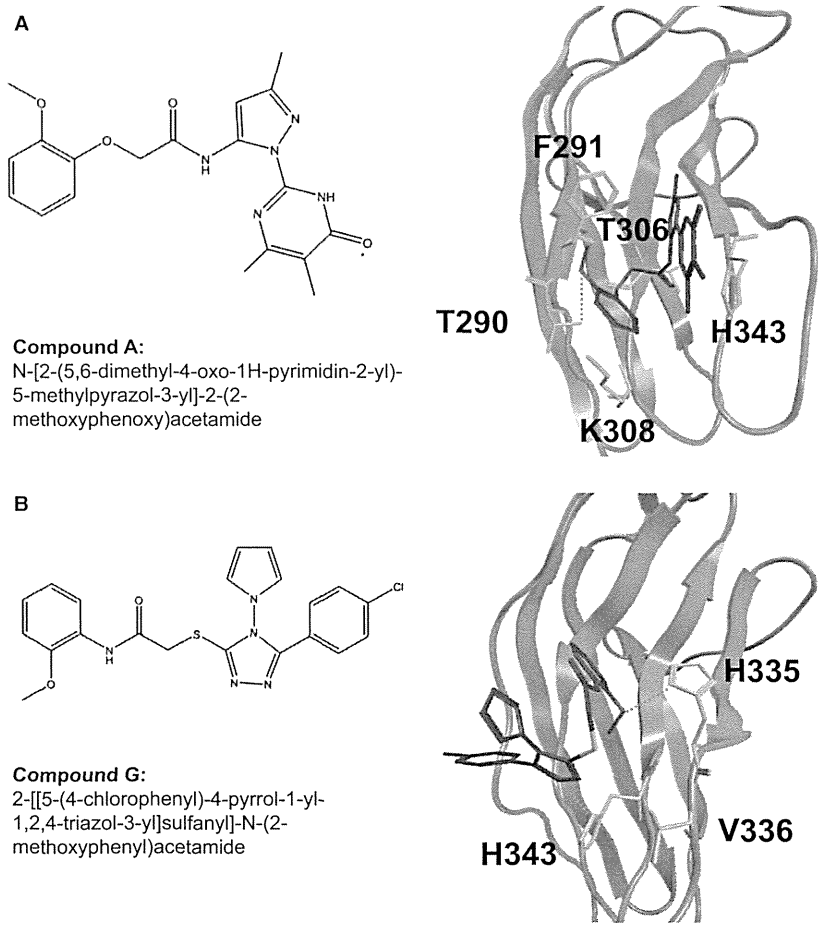

Figure 3. Chemical structure and hypothetical binding model between the molecules A (A) or G (B) and the surrounding residues of TrkB. Amino acid residues involved in the interaction were predicted by the docking simulation.

effect on cell growth. The cell invasion assay demonstrated that the inhibitory effect on cellular invasion mediated by the candidate molecules was facilitated in the presence of BDNF (Fig. 4C). Furthermore, we examined whether the candidate compounds can inhibit the phospho-activation of TrkB, which was mediated by BDNF. BDNF induces phosphorylation of TrkB in a dose-dependent manner in SH-SY5Y/TrkB cells, while the phosphorylated TrkB was significantly decreased by the addition of compound G in the concentration of 100 μmol/L (Fig. 4D), also supporting the notion above.

Candidate compounds induce apoptosis in cell lines and inhibit tumor growth in vivo

Next, we sought to investigate the possible mechanism of the cellular growth inhibition mediated by the candidate compounds. The treatment of CHP134 cells with optimal concentrations of each candidate compound yielded positive signals in the TUNEL assay (Fig. 5A), which is a typical marker of apoptosis in the cells. The stably cloned strain SH-SY5Y/TrkB also demonstrated similar results. Next, whole cell extracts of CHP134 after treatment with the candidate compounds were analyzed using SDS/PAGE followed by Western blotting (Fig. 5B). The compound treatment induced in the cleavage of PARP and caspase 9. Also, the p53 protein was stabilized and phosphorylated at serine 15. These results strongly suggest that the candidate compounds induce apoptosis in the NB cell line. To further prove the biological activity of the candidate compounds, tumor xenograft studies were performed in SCID mice (Fig. 6). Compounds A and G could significantly decrease the size of tumors in mice compared to xenografts treated with mock ($P < 0.05$), suggesting that the candidate compounds exert antitumor activity in vivo. In contrast, the acute in vivo toxicity test (oral and intravenous administrations) using mice has not shown abnormal signs (data not shown) indicating that the cellular toxicity of the candidate compounds to normal tissue is residual.

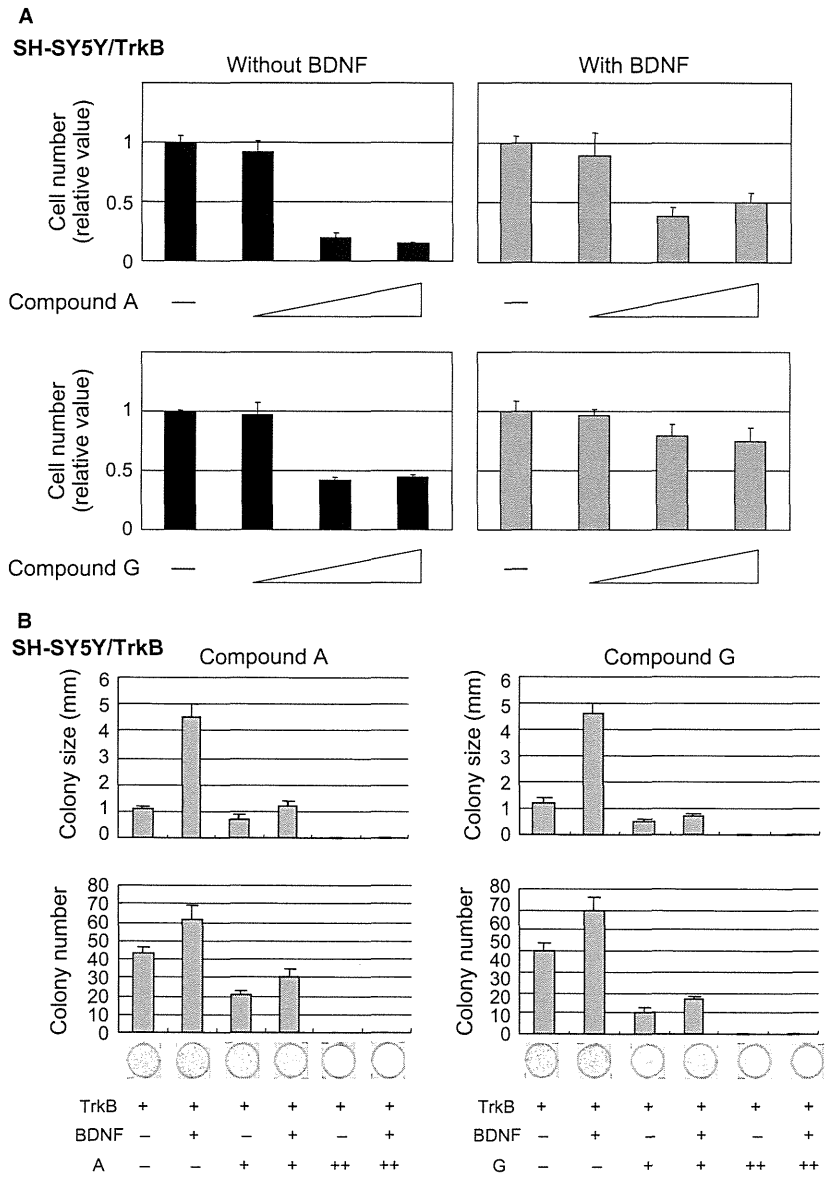

Figure 4. Antagonistic effects of compounds A/G against BDNF in SH-SY5Y/TrkB cells. (A) Growth inhibitory effect mediated by the compounds A and G in the presence or absence of BDNF. The data plotted relative to the cell number without compound (set to 1). Colony formation assay (B) and cell invasion assay (C) indicating an antagonistic effect between the compounds and BDNF. In the cell invasion assay, the data plotted relative to the value at day 0 (set to 1). The *P*-values between the diamond (0 μmol/L) and cross mark (1 μmol/L) at day 5 were less than 0.05 in all experiments except compound A without BDNF (top left panel). (D) The candidate compounds inhibit phospho-activation of TrkB, which is mediated by BDNF. Cells were pretreated with or without compuond G (100 μmol/L) for 5 min, and were incubated with various concentrations of BDNF (0, 5, 15, 25 ng/mL) for 10 min.

Discussion

In this report, we showed that the candidate molecules of anticancer drug could be screened effectively and rapidly by utilizing an in silico docking approach. We identified several molecules that inhibit cellular growth in NB cell lines. The molecular mechanism of this growth inhibition was the induction of apoptosis accompanied by activation of p53 and caspase 9 as well as PARP cleavage. The candidate compounds demonstrated a competitive inhibitory effect against BDNF, a natural ligand of TrkB.

We generated a possible interaction model between the BDNF-binding site of TrkB and small molecules A and G, which are able to induce cellular growth inhibition in NB

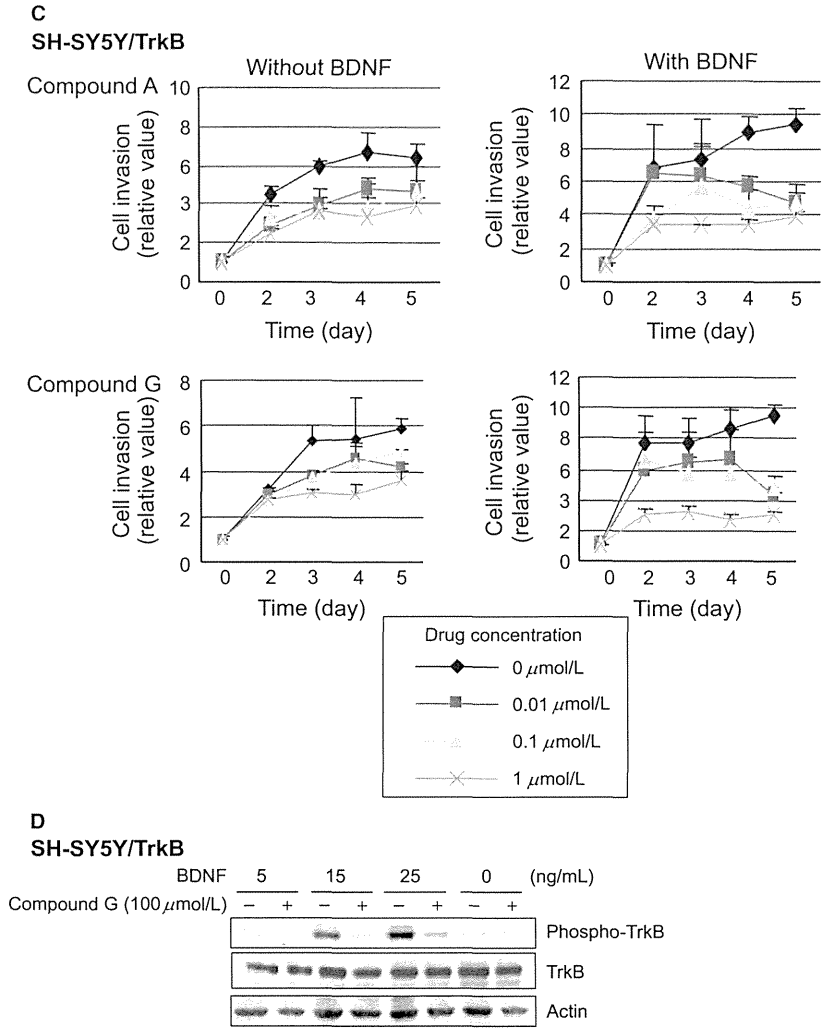

Figure 4. Continued

[21, 22]. The docking simulation with molecule A predicted that the amino acid residues of TrkB, such as T290, F291, T306, K308, and H343, presumably participate in the interaction between TrkB and the candidate molecules (Fig. 3A). Among them, H343 is the only residue that is physically located at the BDNF-binding site. Therefore, we presume that the small molecule A could competitively inhibit the binding of BDNF by forming the π–π interaction with H343. In addition, one of the benzene rings of the molecule A was capable of stabilizing its binding with TrkB by establishing the hydrogen bonds with T290 and T306. Also, the docking simulation with molecule G resulted in the prediction that the residues H335, V336, and H343 of TrkB contribute to the protein-molecule binding (Fig. 3B). In addition, three hydrogen bonds are formed between the molecule G and TrkB (one with H335 and two with H343). We assume that these hydrogen bonds effectively inhibit the interaction between BDNF and TrkB, which may explain the low IC_{50} value of the molecule G.

Because the Trk family of proteins is involved in tumorigenesis, inhibition of tyrosine kinase activity of TrkB has been extensively examined to develop a novel therapeutic treatment in NB [23, 24]. So far, there is no literature reporting an inhibitor specific to TrkB tyrosine kinase activity. Two types of Trk tyrosine kinase inhibitor have been reported. Cephalon's CEP-751 and CEP-701, namely Lestaurtinib, are structural derivatives of staurosporine and are nonselective tyrosine kinase inhibitors that work on several tyrosine kinases such as TrkA, TrkB, TrkC, and protein kinase C. CEP-751 shows potent inhibitory effect on the enzymatic activity of Trks both in vitro and in intact cells. Interestingly, CEP-751 was also found to be without effect when administered to nude mice bearing SK-OV-3 tumors, which overexpress erbB2 receptors, indicating

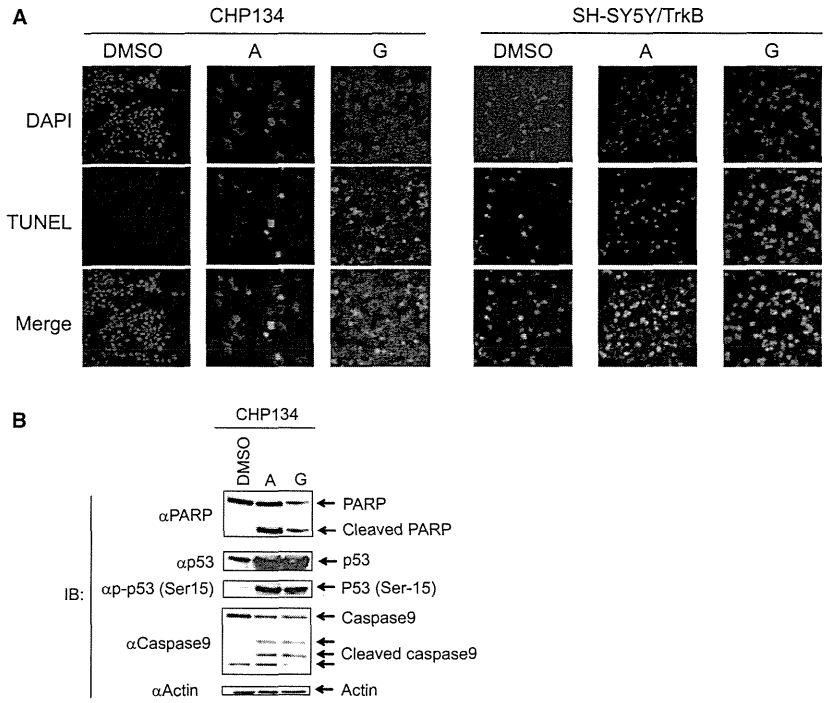

Figure 5. Induction of apoptosis by the candidate compounds. (A) TUNEL assay demonstrating the induction of apoptosis in CHP134 cells. Concentrations of candidate compounds are 5 μmol/L for compounds A and G. Cells were incubated for 3 days prior to TUNEL reaction. DAPI (blue), TUNEL signal (red), and merged images were shown for molecules A and G, respectively. (B) Immunoblotting shows the induction of apoptosis in CHP134 cells. Actin is a loading control.

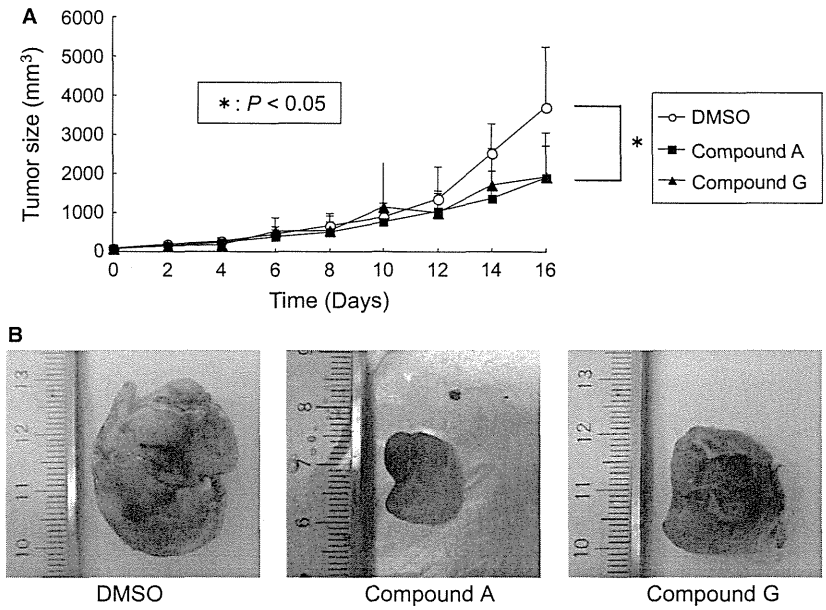

Figure 6. Tumor suppression experiment in vivo utilizing xenografts. (A) When the tumor size reaches to 5 mm square after the injection of CHP134 cells into SCID mice, candidate compounds or mock were treated as described in Material and Methods section. The tumor volume was measured at the indicated days. The data represent the mean value and the error bar represent standard deviation. (B) Representative pictures of tumors obtained at the 20th day after starting administration of the chemicals are shown.